Characterization of Emergent Defects in Retinal Morphology and Gene Expression in dCas9-SPH Transgenic Animals

By

Gökçe Güldöşüren

Submitted to the Graduate School of Engineering and Natural Science

In partial fulfillment of the requirements for the degree of

Master of Science

Sabanci University

December 2024

Abstract

Mouse genetics plays a crucial role in biomedical research, particularly in the generation of transgenic animals. These genetically modified animal models are essential for mimicking human eye diseases, to study disease mechanisms and potential treatments. A novel tool in the development of these models is CRISPR-Cas9, which enables targeted gene modifications to generate disease models. In addition, mutant variant of Cas9, the dead cas9 (dCas9) are also capable of modulating gene expression without cutting the DNA sequences which further enables to study gene regulatory mechanisms. Using this approach, researchers developed a novel transgenic mouse model, the dCas9-SPH (SunTag-p65-HSF1), which utilizes a dCas9 fused to an activator protein to upregulate specific target genes via guide RNAs. Unexpectedly, the homozygous state of this transgenic animal model exhibited an abnormal morphology around the optic disc. This raised a potential opportunity to mimic a disease model related to the glaucoma since this model showed similar characteristics to the optic cupping which occurs in the late stages of glaucoma. Here, we described and characterized this phenotype. dCas9-SPH homozygous animals exhibited persistent optic cupping, despite the absence of increased intraocular pressure (IOP). Retinal ganglion cell (RGC) markers were analyzed, revealing no RGC degeneration. Comparisons with models exhibiting RGC degeneration confirmed this finding. The absence of IOP but presence of optic cupping suggests this model may be used as a hereditary optic cupping model. Notably, GFP leakage in the animal model was observed, indicating activator protein leakage. ddPCR analysis implicated Dpysl2 gene knockdown from insertional mutagenesis as the most likely cause of the phenotype. These findings highlight the potential of the homozygous dCas9-SPH animals to contribute to our understanding of genetic factors in optic nerve diseases.

Gökçe Güldöşüren

Molecular Biology, Genetics and Bioengineering, MSc Thesis, December 2024

Thesis Supervisor: Asst.Prof. Cavit Agca

Keywords: Glaucoma, dCas9-SPH, Gene regulation, Optic cupping, Dpysl2, ddPCR

Özet

Mouse genetiği, özellikle transgenik hayvanların üretilmesinde biyomedikal araştırmalarda kritik bir rol oynar. Bu genetik olarak değiştirilmiş hayvan modelleri, insan göz hastalıklarını taklit etmek, hastalık mekanizmalarını ve potansiyel tedavileri incelemek için gereklidir. Bu modellerin geliştirilmesinde yenilikçi bir araç olan CRISPR-Cas9, hedef gen değişikliklerini mümkün kılarak hastalık modelleri oluşturulmasını sağlar. Buna ek olarak, Cas9'un mutant bir varyantı olan "dead Cas9" (dCas9), DNA dizilerini kesmeden gen ekspresyonunu modüle edebilme yeteneğine sahiptir ve bu da gen düzenleyici mekanizmaların incelenmesini sağlar. Bu yaklaşımı kullanarak, araştırmacılar dCas9-SPH (SunTag-p65-HSF1) adlı yenilikçi bir transgenik fare modeli geliştirmiştir. Bu model, belirli hedef genlerin kılavuz RNA'lar aracılığıyla regüle edilmesi için dCas9'un bir aktivatör proteine füzyonunu kullanmaktadır. İlginç bir şekilde, bu transgenik hayvan modelinin homozigot durumunda, glokoma benzer bazı özellikler gözlemlenmiştir. Bu durum, glokoma ile ilgili bir hastalık modelini taklit etme potansiyelini ortaya çıkarmıştır çünkü bu model, glokomanın ileri evrelerinde görülen optik çukurlaşmaya benzer özellikler göstermiştir. Bu çalışmada, bu fenotip tanımlanmış ve karakterize edilmiştir. Artan göz içi basıncı (IOP) olmamasına rağmen, modelin kalıcı optik çukurlaşma sergilediği gösterilmiştir. Retinal ganglion hücresi (RGC) belirteçleri analiz edilmiş ve RGC dejenerasyonu bulunmamıştır. RGC dejenerasyonunun gözlemlendiği diğer modellerle yapılan karşılaştırmalar, bu bulguyu doğrulamıştır. Göz içi basıncının olmaması ancak optik çukurlaşmanın varlığı, bu modelin kalıtsal

bir optik çukurlaşma modeli olarak kullanılabileceğini göstermektedir. Önemli olarak, hayvan modelinde gözlemlenen GFP sızıntısı aktivatör proteinin sızdığını gösterdi. Ancak, ddPCR analizleri fenotipin nedeninin eklemeli mutagenezden kaynaklanan Dpysl2 geninin baskılanması olduğunu ortaya koydu. Bu bulgular, bu dCas9-SPH fenotipinin optik sinir hastalıklarındaki genetik faktörlerin anlaşılmasına katkıda bulunma potansiyelini vurgulamaktadır.

Gökçe Güldöşüren

Moleküler Biyoloji, Genetik ve Biyomühendislik, Yüksek Lisans Tezi, Aralık 2024

Tez Danışmanı: Dr. Cavit Agca

Anahtar Kelimeler: Glokom, dCas9-SPH, Gene regülasyonu, Optik çukurlaşma, Dpysl2, ddPCR

ACKNOWLEDGEMENTS

I hereby thank my supervisor Assistant Professor Cavit Ağca, who always eagerly shared his limitless scientific guidance with patience and as he always supported me as a master student during my whole master process. With his academic achievements and attitude towards his colleagues and students, he is definitely a role model for my future career path.

I would like to thank to my husband and mother for their loving care and support towards me unconditionally in every stage of my life.

I would like to thank my lab-mates, İskalen Cansu Okan, Mehri Ahmadian and Halit Yusuf Altay, for making my time in Sabancı University much more easier and fun.

I would like to thank Assistant Professor Stuart James Lucas and Associate Professor Markus Tschopp for taking their time and being my jury members and their support.

Last but not least, I would like to thank Acıbadem Mehmet Ali Aydınlar University employees for giving us support and opportunity to hold animal experiments in their facilities.

TABLE OF CONTENTS

1. INTRODUCTION 12
   1.1. The Vertebrate Eye and Retina 12
   1.2. Degenerative Eye Diseases 16
   1.3. Glaucoma 18
   1.4. dCas9-SPH Mouse 24
2. MATERIALS AND METHODS 27
   2.1. Animal Breeding Strategy 27
   2.2. Breeding Strategy of dCas9-SPH Transgenic Mouse 28
   2.3. Generation of Pou4f1$^{AP/AP}$ Transgenic Mouse 29
   2.4. Genotyping 30
      2.4.1 Toe Biopsy 30
      2.4.2 PCR Genotyping 31
         2.4.2.1 dCas9-SPH PCR 31
         2.4.2.2 Pou4f2 PCR 34
      2.4.3 Agarose Gel electrophoresis 36
   2.5. Retina Isolation 37
      2.5.1 Whole Retina Isolation and Total RNA Isolation from Retina 37
      2.5.2 Whole Retina Isolation and Dissociation 38
   2.6. NanoDrop Analysis 39
   2.7. Assessment of gRNAs in vitro 39
      2.7.1 cDNA Synthesis 39
      2.7.2 Digital Droplet PCR (ddPCR) 40
   2.8. *In vivo* Imaging Techniques 42
      2.8.1 MicronIV Retina Fundus and Fluorescence Imaging 42
      2.8.2 Optical Coherence Tomography (OCT) 44
   2.9. pAAV-sgRNA Vector Design 44
3. RESULTS 45
   3.1 Analysis of Retinal Integrity and GFP Leakage Across Genotypes 45
   3.2 Intraocular Pressure Assessment Across Genotypes 49
   3.3 ddPCR-Based Analysis of Retinal and Neurodegenerative Gene Expression 51

3.4 Genotypic Analysis of dCas9-SPH Variants and Correlation with Optic Cupping Phenotype 54
3.5 Integration of dCas9-SPH in Dpysl2 Gene and Its Potential Knockout Effect 55
4. DISCUSSION 58
5. BIBLIOGRAPHY 63

LIST OF FIGURES

Figure 1. The simplified cartoon of the eye`s anatomical features 13
Figure 2. Simplified version of retina anatomy and neuronal network 16
Figure 3. Mechanism for secondary cone degeneration 18
Figure 4. Schematic cartoon of Optic Nerve Cupping 20
Figure 5. Breeding strategy for dCas9-SPH transgenic mouse line 29
Figure 6. Representative Gel Image of dCas9-SPH PCR with Suntag primers 33
Figure 7. Representative Gel Image of dCas9-SPH PCR with wild-type primers 34
Figure 8. Representative Gel Image of Pou4f2 PCR with AP primers 36
Figure 9. Cre-dependent SPH transgenic mouse 47
Figure 10. Fundus and OCT features of dCas9-SPH mice 47
Figure 11. Flow cytometry analysis of dCas9-SPH retinas. 49
Figure 12. IOP measurements from three different genotypes 50
Figure 13. Primer testing for different genotypes 54
Figure 14. Primer testing for Dpysl2 gene between genotypes 58

LIST OF TABLES

Table 1. Lysis buffer 30
Table 2. Neutralization buffer 30
Table 3. GoTaq Green Master Mix 31
Table 4. Standard PCR reaction 32
Table 5. dCas9-SPH Touchdown PCR Amplification 32
Table 6. Pou4f2 AP PCR Amplification 35
Table 7. List of Primers For PCR Genotyping of dCas9-SPH and Pouf2 animals 36
Table 8. Standard cDNA Synthesis. Preparation of the standard cDNA synthesis. 40

Table 9. List of Primers For ddPCR Gene Expression Analysis of Pou4f1, Melanopsin, NfL, Rho Dpysl2 and Gapdh gene analysis 42
Table 10. Mouse genotypes checked with PCR, MicronIV and OCT 55

LIST OF ABBREVIATIONS

AMD: Age-Related Macular Degeneration

BSG1: Basigin-1

Cas: CRISPR-Associated Endonuclease

cDNA: Complementary DNA

Crmp2: Collapsin Response Mediator Protein 2

crRNA: CRISPR RNA

ddPCR: Digital Droplet PCR

dNTP: Deoxynucleoside Triphosphate

DNA: Deoxyribonucleic Acid

DPYSL2: The Dihydropyrimidinase-Like 2

EDTA: Ethylenediaminetetraacetic Acid

EGFP: Enhanced Green Fluorescent Protein

FACS: Fluorescence-Activated Cell Sorting

GCL: Ganglion Cell Layer

GFP: Green Fluorescent Protein

GFAP: Glial Fibrillary Acidic Protein

GLUT1: Glucose Transporter Type 1

gRNA: Guide RNA

ILS: Photoreceptor Inner Segments

INL: Inner Nuclear Layer

IOP: Intraocular Pressure

IPL: Inner Plexiform Layer

IRD: Inherited Retinal Diseases

LSL: Lox-Stop-Lox

MGE: Mobile Genetic Element

MGS: Morning Glory Syndrome

$MgCl_2$: Magnesium Chloride

mCherry: Monomeric Cherry

mRNA: Messenger RNA

Mtor: Mechanistic Target Of Rapamycin

Myoc: Myocilin

NFL: Nerve Fiber Layer

NTG: Normal Tension Glaucoma

OCT: Optical Coherence Tomography

OLS: Photoreceptor Outer Segments

ONL: Outer Nuclear Layer

Opn4: Melanopsin

OPL: Outer Plexiform Layer

PAM: Protospacer Adjacent Motif

PCG: Primary Congenital Glaucoma

P2A: Porcine Teschovirus 2A Peptide

PCR: Polymerase Chain Reaction

PND: Postnatal Day

POAG: Primary Open-Angle Glaucoma

RA: Retinoic Acid

RdCVF: Rod-Derived Cone Viability Factor

RGC: Retinal Ganglion Cell

Rho: Rhodopsin

RNA: Ribonucleic Acid

RNFL: Retinal Nerve Fiber Layer

RP: Retinitis Pigmentosa

RVDs: Repeat-Variable Di-Residues

sgRNA: Single Guide RNA

SPH: SunTag-P65-HSF1

T2A: Thosea Asigna 2A Peptide

TAE: Trisaceticacid EDTA

TALENs: Transcription Activator-Like Effector Nucleases

TIGR: Trabecular Meshwork Inducible Glucocorticoid Response

TM: Trabecular Meshwork

Tbk1: TANK Binding Kinase1

WDR36: WD Repeat Containing Protein 36

YFP: Yellow Fluorescent Protein

ZNF: Zinc-Finger Nucleases

1. INTRODUCTION

1.1. The Vertebrate Eye and Retina

Animals obtained the capacity to perceive and encode their environment via evolution. Through evolution they develop different sensory systems such as touch, audition, olfaction and vision [1]. Vision is the most predominant sense for many vertebrates for environmental information. The main function of the eye is focusing the outer light. Eyes are responsible to sense light, transform it into neuronal electro-chemical signals and process the visual information. There are different parts of the mammalian eye such as cornea, the translucent part of the mammalian eye shown in **figure 1**. Cornea allows the outer light pass through and also protects the pupil [2]. There is also iris which is the colored part, placed behind the cornea. The function of iris is expanding and contraction the pupil as light exposure change. Sclera, uvea and retina are the three concentric and distinct layers of mammalian eye. Retina functions through the phototransduction cascade. Phototransduction is the process of delivering information to the brain with converting light energy into encoded neural signals. It is performed with neurons and with the support of glial cells contained by the laminar tissue [1]. Some mammals like humans have macula which contains high amounts of ganglion cells and cones since it is characterized for color and detailed vision. However, rodents do not have macula or fovea which is another feature that needs to be considered for human studies [3].

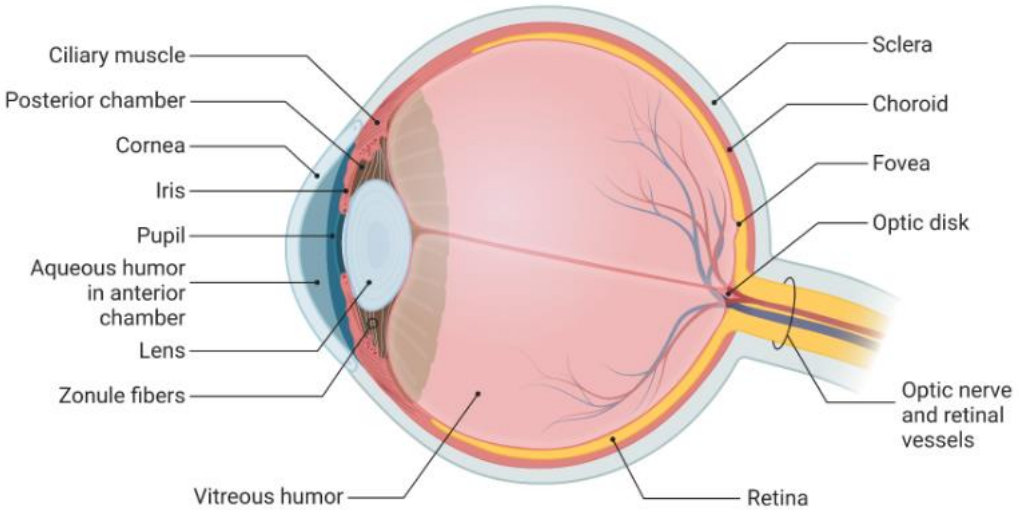

Figure 1. The simplified cartoon of the eye`s anatomical features. *Eye have three distinct layers called external layer, intermediate layer and inner layer. External layer contains sclera and cornea; intermediate layer contains the choroid and ciliary body; inner layer contains the retina. Ciliary muscles and zonule fibers are helpful for changing the shape of crystalline lens while cornea is a stationary lens. Anterior and posterior chambers fill the space between cornea and iris, and iris and lens, respectively, and they filled with aqueous humor. Iris restricts the light to access retina through pupil by blocking the light. Cornea covers both the iris and pupil. Vitreous humor fills the eye interior. Fovea is the cone exclusive region and macula is the cone rich region surrounding fovea; both located in retina. Light signal transportation is occurring via retinal ganglions cells to the brain through optic nerve. The surrounding around the optic nerve is called optic disc. Figure adapted from "Anatomy of the Human Eye", by BioRender.com (2022). Retrieved from https://app.biorender.com/biorender-templates*

There are five different classes of neurons in the human retina specialized in processing the visual information. Photoreceptors, ganglion cells, bipolar cells, amacrine cells and horizontal cells are

the neuronal types [1]. These neurons distributed through the ten distinct layers of the human retina The layer of rods and cones, The retinal pigment epithelium (RPE), External limiting membrane, Outer nuclear layer, Outer plexiform layer, Middle limiting membrane, Inner nuclear layer, Inner plexiform layer, Ganglion cell layer, Nerve fiber layer (NFL), Inner limiting membrane [4] and eight distinct layer-layer aggregates in mouse retina, The retinal pigment epithelium (RPE), Photoreceptor outer segments (OLS), Photoreceptor inner segments (ILS), Outer nuclear layer (ONL), Outer plexiform layer (OPL), Inner nuclear layer (INL), Inner plexiform layer (IPL), and Retinal nerve fiber layer and Ganglion cell layer complex (RNFL-GCL), according to their characteristics and has interconnections with vertical and horizontal pathways [5] shown in **figure 2**. Through the extensive interconnections of these neurons, they enable to process the visual image projected on the retina and they can transfer the information to the brain with the optic nerve through retinal ganglion cells (RGCs). Transduction of light signals by the photoreceptors and transmission with the RGCs axons to the brain is regulated by the vertical pathway. Horizontal pathway on the other hand provides feedback and feedforward signals between bipolar cells and photoreceptor cells and also between RGCs and bipolar cells [1].

Retinal ganglion cells which are thought to have 20 subtypes in the mouse are the output neuron of the eye. Function of the RGCs are conveying retinal visual information through the optic nerve to the brain. In the brains it aims a variety of functionally different areas [6]. Retinal ganglion cell axons move to the lateral geniculate nucleus for visual perception. RGCs pass through the suprachiasmatic nucleus for circadian rhythm regulations [7]. Some of the retinal ganglion cell axons terminates the pretectal area for the pupillary light reflex [8]. Retinal ganglion cells process the information they take from the retina and convey it to the visual centers of the brain. Almost all retinal ganglion cells share the same morphology with some exceptions such as the size of their

dendritic field and stomata and their dendritic architecture and axonal projection patterns that can strikingly vary [9-12]. There are different ways a retinal ganglion cell response to light such as tonic or phasic, brisk or sluggish, transient or sustained. Some RGCs may adopt a unique direction for the movement of the stimulus for detecting motion, on the other hand some other RGCs are delicate to the orientation of the stimulus not the direction of the stimulus [13].

Gradual loss of RGCs is the pathophysiological hallmark of glaucomatous optic neuropathy [14]. RGCs found in the central nervous system are just like other neuron types and once they die, they are lost forever [15]. Glaucoma is a complex multifactorial disease, therefore, progression of glaucoma can be linked to some risk factors , such as age, elevated intraocular pressure, vascular dysregulation and thinner corneal thickness [16]. These risk factors may exacerbate the signals that promote RGC death in glaucoma and cause the dysfunction and demise of the cells [17].

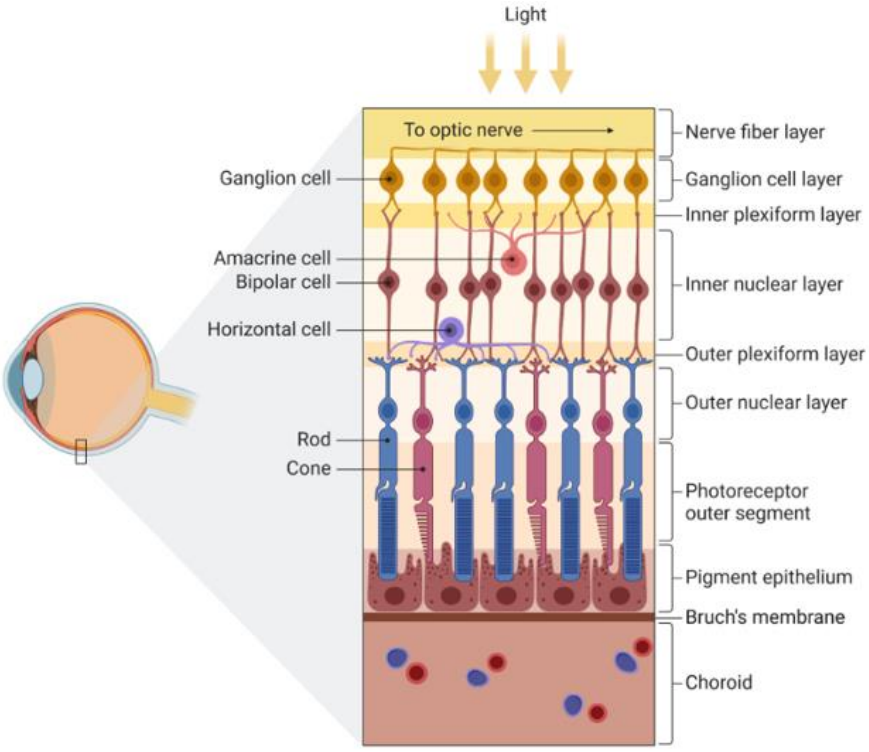

Figure 2. Simplified version of retina anatomy and neuronal network. *Light hits the retina and moves to the photoreceptor layer through inner layers. Photoreceptor layer contains rod and cone opsin proteins which absorbs the incoming light. Axons of RGCs moving towards the optic nerve obtained in the nerve fiber layer which is the innermost layer. RGC, bipolar and amacrine cells make connections in the IPL. INL contains bipolar, Müller, amacrine and horizontal cell bodies. In the OPL, synapses are made by photoreceptor cell axons and INL neurons. Photoreceptors cell bodies are located in the ONL. Inner and outer segments of photoreceptor cells reside in the photoreceptor layer. RPE cells supports photoreceptor cells and contained by the RPE layer. Retina is separated from the choroid by Bruch's membrane at the outermost part of the eye. Figure adapted from "Structure of the Retina", by BioRender.com (2022). Retrieved from https://app.biorender.com/biorender-templates*

1.2. Degenerative Eye Diseases

Vision plays a curial ability for a living beings' growth and survival. Vision damage alters the mobility and independence of a person and normal daily life [18]. Vision loss also put an economic burden, for example in United States in 2017 the estimated cost for vision lost is over 134 billion. The variation in total burden is driven primarily by age composition and the population size of the state [19].

The human eye is a very sophisticated organ which has one significant focus, a clear image of the visual world upon retina [20]. Retina converts light energy into neuronal action potentials with a chemical reaction and it is involved in the Central Nervous System. Two types of photoreceptor cells rods and cones perform this chemical reaction. They are placed in the outer retinal layer adjacent to the retinal pigment epithelium [21].

Vision loss can be caused by many retinal disorders such as, diabetic retinopathy, age-related macular degeneration, glaucoma and inherited retinal disorders [22]. Some ocular pathologies like cataracts, dry eye, myopia, corneal wound healing, retinal diseases and glaucoma can be affected by the circadian rhythm [23]. Diabetic retinopathy is associated with changes in retinal vessels and neuroglia anatomically [24]. Diabetic retinopathy has a variety of progresses, such as, mild non-proliferative abnormalities to moderate and severe non-proliferative diabetic retinopathy and proliferative diabetic retinopathy [25]. Age-related macular degeneration (AMD) is a progressive condition and a leading cause of blindless in the elderly worldwide [22]. AMD can be characterized into two types, dry and wet. Early stages of AMD is asymptomatic, but there is an accumulation of drusen in the retina. The last stage of dry AMD is characterized by degeneration in the RPE cells that are scattered or confluent [26]. The late stage of wet AMD is characterized by growing of new blood vessels toward the outer retina from the underlying choroid called choroidal neovascularization [27].

Inherited retinal diseases (IRD) is a group of disorders that are mostly genetically heterogeneous in humans. It affects almost 2.5 million people worldwide. Retinitis Pigmentosa (RP) has been linked to over 3,000 genetic mutations across approximately 70 genes, along with significant genetic overlap with other retinal dystrophies [28]. Inherited Retinal Disease (IRDs) can be inherited as autosomal dominant, autosomal recessive or X-linked [28]. Retinitis pigmentosa is described with primary loss of rod photoreceptors, then secondary loss of cone receptors**.** First symptom of this degenerative process is gradual vision loss function, and it can eventually end up with more advanced stages in visual function [29].

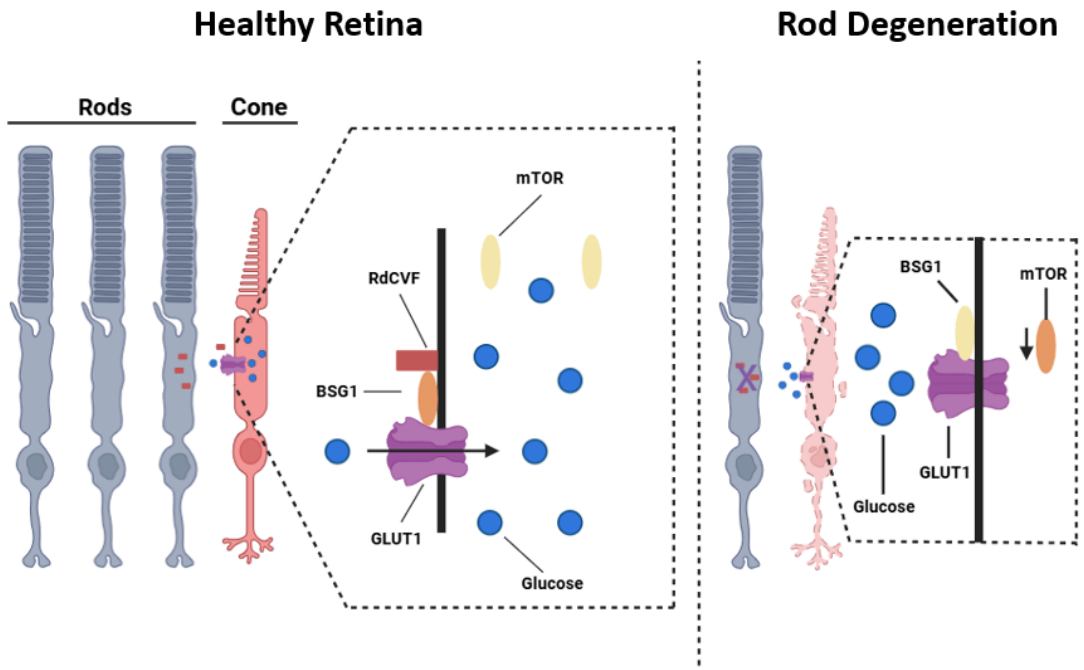

Figure 3. Mechanism for secondary cone degeneration. *In healthy retina, rods bind to BSG1 and produce RdCVF to support cone function which allows GLUT1 receptor to open and help the glucose to enter the cones. In the case of a disease where rods are degenerated; cone GLUT1 receptor remains inactive since the RdCVF is no longer produced. Therefore, cones begin to degenerate secondary to the loss of rods because dysregulation of glucose uptake into cones causes a decrease in Mtor. Figure adapted from https://pmc.ncbi.nlm.nih.gov/articles/PMC8775779/. [30] Figure generated on https://app.biorender.com/*

1.3. Glaucoma

Glaucoma is an irreversible eye disease. It can affect 70 million people worldwide [31]. Group of disorders can be categorized as glaucoma with a range of different pathophysiology, prognoses,

risk factors and treatments. Important risk factor of glaucoma is increase in the intraocular pressure. Its common indicator due to loss of RGCs is, thinning of the retinal nerve fiber layer and progressive optic nerve degeneration [32]. Glaucoma is a complex disorder; different stresses may affect RGCs [33]. Major risk factors of glaucoma are family history, age and elevated intraocular pressure (IOP). IOP regulation itself is a complex situation in most glaucoma cases and thus it is not clear [34]. Various studies showed that mouse models are useful for glaucoma relevant aspects of the anterior segment physiology, over the last decade. Moreover, human and mouse have similar cyclical IOP patterns [35]. Another similarity between mice and humans are the mutations that lead to anterior segment diseases. Humans and mice have similar mechanisms regulating aqueous humor production and outflow; similar response to IOP lowering drugs which are the key physiological parameters for IOP regulation [36]. Therefore, for studying glaucoma relevant anterior segment physiology and pathophysiology, mouse is a beneficial model system[37].

Mouse glaucoma models are limited to ocular hypertension-induced RGC degeneration studies since optic nerve head structure and morphology is different between humans and mice [15, 38]. Mouse optic nerve has pores created by optic nerve head astrocytes instead of collagen beams [39]. Optic nerve head is a key site in ocular hypertensive glaucoma, therefore the differences in optic nerve head morphology may limit the studies for ocular hypertension-induced optic neuropathy with mouse modelling [40]. However, recent findings related to the ocular hypertension-induced RGC death showed many hallmarks of human hypertensive glaucoma (such as;, ocular hypertension-induced abnormalities in RGC physiology, segmented axon loss. All these phenotypes are also typical features of human glaucoma [15, 34, 41].

The enlargement of the cup to disc ratio shown in **figure 4**, which called optic nerve cupping is extensively recognized feature of the disorder glaucoma, however, in some cases it can also seen

in non-glaucomatous optic neuropathies [42]. Initial histopathological studies showed that, the reason behind the optic nerve cupping phenotype is thinning and the posterior displacement of the lamina cribrosa and loss of retinal ganglion cell axon fibers [43]. The optic cupping phenotype may be related to non-glaucomatous processes or can be physiologic. Other recognized disorders that can show optic cupping are hereditary optic neuropathies, arteritic anterior ischemic optic neuropathy, and compressive optic neuropathies. Well known reasons for the non-glaucomatous optic cupping are with greater neuroretinal rim pallor and less profound excavation than seen in glaucoma and often has different visual manifestations [44].

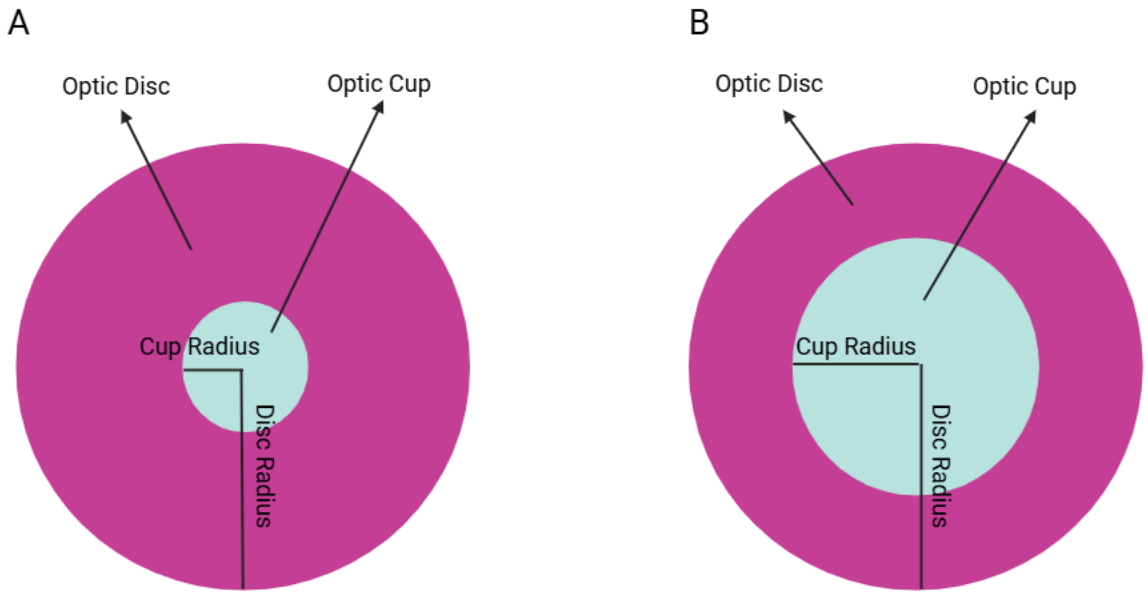

Figure 4. Schematic cartoon of Optic Nerve Cupping. ***A)*** *Shows a healthy retina.* ***B)*** *Shows a retina with Optic Cupping, with the enlargement of the cup to disc ratio. Figure generated on https://app.biorender.com/*

There are some genes and proteins that has been shown to be associated with glaucoma such as *Myoc (Myocilin), Optn (Optineurin), Cyp1b1, Tbk1 (TANK Binding Kinase1) and WDR36* (WD Repeat Containing Protein 36). The *Myocilin* gene (*Myoc*), encodes a secreted protein called myocilin. *Myoc* gene was also known as trabecular meshwork-inducible glucocorticoid response (TIGR) gene [45], was the first discovered gene to be linked to POAG in 1997[46]. *Myoc* is detected in the aqueous humor and mutations of *Myoc* are the most frequent form of mutation in patients with glaucoma [47], found in 10% of juvenile-onset open-angle glaucoma (JOAG)[48] and 2-4% of adult-onset POAG [49]. *Myocilin* is highly expressed gene in the trabecular meshwork (TM). The important role of Myocilin is the regulation of IOP. Abnormalities on the *Myocilin* gene can alter the function of TM, and can subsequently cause the elevation of IOP which is one the risk factors of glaucoma [50].

Optn (Optineurin gene) is the second gene that the mutations of it have been associated with POAG beside *Myoc* [51]. *Optn* is a multifunctional protein which mediates autophagy and different vesicle and signaling pathways. It is expressed in both mice and humans, the cells and tissues it is expressed in are retina, liver, hearth and brain[52]. Normal tension glaucoma (NTG) is a considerable subtype of POAG is linked with increased IOP and *Optn* was the first gene to be detected in which the mutations of it are associated with NTG. M ostly missense mutations of *Optn* are glaucoma related mutations [53]. Variety of *Optn* missense mutations have been reported that are associated with glaucoma, such as E322K, H486R, H26D and E50K [54]. Transgenic mice which express E50K-OPTN have been created. This transgenic mouse showed RGC loss and weakening of different cell layers of retina [55-57]. This mouse model is particularly advantageous for studying NTG, as it does not exhibit elevated IOP [54].

Primary congenital glaucoma (PCG) is a recessively inherited disorder of the eye with variable penetrance. It affects the anterior chamber angle and the trabecular meshwork which causes the blocking of the outflow of aqueous humor, elevated IOP and damage in the optic nerve [58]. Pathogenic variations in the *Cyp1b1* gene were first associated with PCG. This condition is inherited in an autosomal recessive fashion, which leads to a much rare condition than POAG [59]. *Cyp1b1*is a monooxygenase, which catalyzes many reactions involved in the metabolism of endogenous compounds [60]. *Cyp1b1* gene has a role in metabolizing retinoic acid (RA), and RA is important for ocular development. The dysfunction in the *Cyp1b1* gene can alter RA metabolization which can implicate the cause of PCG [60, 61]. Another relation between *Cyp1b1* gene and glaucoma is dysfunction in the 17β estradiol metabolizing activity of some mutants of *Cyp1b1* can cause *Myoc* upregulation and upregulation of *Myoc* can lead to POAG pathogenesis [62] mentioned above.

Tbk1 encodes a kinase protein which directly phosphorylates and interacts with *Optn* [63]. *Tbk1* is mostly affected by normal tension glaucoma (NTG) and it is specifically expressed in the ocular tissue and the RGC layer [64]. Normal tension glaucoma has features similar to POAG, only difference is the absence of the increased IOP [65]. Duplication and triplication on *Tbk1* gene mutations on chromosome 12q14 results in a significant increase in the level of transcription in *Tbk1* which indicated *Tbk1's* involvement in the progression of glaucoma pathology [66]. Because *Tbk1* is the only gene encompassed by all known chromosome 12q14 duplications in NTG patients [67].

Wdr36 is another gene associated with glaucoma that encodes the protein WD repeat domain 36 and located on 5q22.1, is detected as the causative gene of adult onset POAG [68]. *Wdr36* mRNA depletion in human trabecular meshwork cells causes the upregulation of several mRNAs,

including p53 and apoptotic cell death [69]. Studies on zebrafish have demonstrated that the loss of function of Wdr36 activates the p53 stress response pathway. This information suggests that coinheritance of defects in genes of this route may modify the impact of *Wdr36* variants on POAG [70]. P53 is a tumor suppressor gene that encodes a transcription factor which activates gene expressions involved in growth arrest or apoptosis in response to multiple forms of cellular stress [71].

Developing a treatment for monogenic disorders can enable scientists to focus on a handful of targets. However, treating diseases like Parkinson's and Alzheimer's which are multifactorial disorders can be quite difficult [72]. Glaucoma is a multifactorial disease. The most common type of glaucoma is Primary open-angle glaucoma (POAG) and a proof-of-concept study was demonstrated with CRISPR-mediated gene correction for POAG [73].

Morning Glory Syndrome (MGS) is a rarely found congenital optic disc anomaly. This syndrome mostly affects one eye. The characterization of the anomaly is an enlarged, funnel shaped optic disc with the central mass of glial tissue and retinal vessels that appear from the center of the core in radial pattern and expand through the peripheral retina [74]. MGS often appears as an isolated ocular anomaly however it has associations with the systemic anomalies such as central nervous system and kidneys, it is also an untreatable and nonprogressive condition. MGS can also be associated with preretinal gliosis, afferent pupillary defect, congenital cataract, ciliary body cyst, strabismus, presence of hyaloids artery remnants, lid hemangioma and visual field defects such as blind spot enlargement and central scotomata [75-77].

1.4. dCas9-SPH Mouse

Gene modification tools are essential to the landscape of molecular biology [78, 79]. Previously, modifying genomes was highly challenging. However, it has now become significantly easier and more feasible to modify genomes in specific regions, enabling targeted recombination within cells to alter genomic loci [80]. It is also possible to use them as a gene regulatory tool with dCas9 versions [81]. For ophthalmology; gene editing, gene replacement and other gene regulatory treatments are expanding in terms of complexity, numbers and approval of therapies. Translational research on gene therapy is more convenient for the eye since compared to other organs, eye has exceptional properties. First, it is very small therefore microsurgery techniques are easy to perform. Furthermore, the systemic effects of the treatment is reduced since eye is an isolated organ. Finally checking the treatments effects with imaging is easy to accomplish because eye is a very accessible organ [72, 82, 83].

There are two different types of genome editing tools, first one is RNA-guided endonucleases such as clustered regularly interspaced short palindromic repeats (CRISPR) and CRISPR-associated (Cas) systems. Second one is artificial nucleases, such as zinc-finger nucleases (ZFNs) and transcription activator-like effector nucleases (TALENs). All of these tools can induce double stranded breaks and the following repair systems could introduce mutations to selected sites [84]. Cas9 is an RNA-guided endonuclease that can directly cut a targeted site. This process needs complementarity between the selected site and the Cas9 associated gRNA in addition to the presence of a short protospacer adjacent motif (PAM) [78, 79, 85, 86]. Initial studies for the Cas9 protein engineering disclosed several residues involved in DNA catalysis that, when mutated, can create protein forms that are still capable of DNA binding but lack detectable nuclease activity [79, 87, 88]. These dead or nuclease-null Cas9 variant (dCas9) can then be fused to effector domains.

This fusion enables researchers to specifically direct a given functional activity to any arbitrary locus within the genome [87, 89-91]. The advantages and disadvantages of dCas9 are, dCas9 gene editing allows multiplexing when the presence of a gRNA and also rapid screening [81, 92]. However, the disadvantage is the dependency to the PAM sequence and also the large size of the dCas9 [78, 79]. Also, since it is bacterial-derived system it can trigger inflammation [86, 93].

Zinc-finger nucleases (ZFNs) and transcription activator-like effector nucleases (TALENs) are other gene editing tools other than dCas9 [94]. ZNFs are composed of a designed polymeric zinc finger domain precisely for target sequence of a DNA and FokI nuclease cleavage domain [95-101]. For cutting the DNA FokI needs dimerization. The result of FokI dimerization and subsequent DNA cleavage is by binding of two heterodimers of designed ZFN-FokI hybrid molecules to two contiguous target sequences in each DNA strand separated by a 6 base-pair cleavage site [102]. Polymeric zinc finger domains are the DNA binding properties of which are generated through modular assembly of individual zinc fingers, determine the specificity of ZNFs [103, 104]. Zinc finger nucleases are smaller in size and of human origin which reduces inflammation risks. However, the screening process is very complex compared with other gRNA-based systems [105].

TALENs are designed as sequence-specific DNA-binding domains and non specific DNA cleavage module [94]. Transcription activator-like effector (TALE) proteins serve as novel DNA-binding domains and originally found in plant pathogen [106-108]. TALE consists of a central region. Central region obtains an array of 33- to 35-amino acid-repeat module. The amino acid sequences of each repeat are almost exact except for the adjacent amino acids (the repeat-variable di-residues or RVDs) [108-110]. In the targeted DNA sequences and repeat domains there is one-to-one correspondence between the RVDs [106, 108]. For cutting the desired sequences and create a DBS

FokI is artificially fused to DNA-binding domains [109, 111]. TALENs are more flexible compared to Cas9 since they do not require a PAM sequence. Just like dCas9, TALENs are also in the larger size which reduces efficiency. Another limitation of TALENs is they have a complex cloning process because they require a separate domain corresponding to each nucleotide in the target sequence [106]. Given these considerations, the use of CRISPR-Cas9 is more common with its easy to design gRNAs, capacity for multiplexing and rapid screening capabilities over other gene editing tools [80].

CRISPR-Cas9 proteins discovery bring a new perspective to science. It has a broad spectrum in fields from bioimaging to genetics. The beneficial parts of this system are, it is very practical, has a reduced cost compared to other technologies, and adaptable to multiple situations. In nature, CRISPR-Cas9 systems are elements of bacterial and archaeal adaptive immunity against invasive mobile genetic elements (MGEs) [112]. CRISPR-associated endonuclease (Cas) cleaves invading MGEs. To recognize the target sequence from invader MGEs, native forms of CRISPR-Cas systems require CRISPR RNA (crRNA). CrRNA identifies protospacer adjacent motifs (PAMs) which are kept in MGEs, with that it recognizes target sequences. When the recognition event occurs, cleavage silences the genetic elements of the invader. Integration of invader DNA sequences into the CRISPR loci enables immune memory of past infections [113]. Prokaryotic immune system components have a high diversity; therefore, they are very beneficial for diverse applications such as molecular diagnostics and gene editing. This system is very advantageous for gene editing for inherited retinal diseases since it has high versatility and very cost effective. CRISPR-Cas9 systems offer numerous opportunities for future therapeutics for IRDs from artificial transcriptional networks to RNA editing and gene knockouts [72].

Zhou et al. aimed to develop a robust transcription activation domain and focused their work on the VP64 transcription activation domain. They substituted VP64 in SunTag with p65-HSF1 transcription factors, utilized within the Synergistic Activation Mediator (SAM) system. They made this replacement because GCN4 transcriptional activator repeats can induce more potent transcriptional activation when combined with multiple copies of p65-HSF1 [114]. Zhou et. al study group generated the SPH transgenic mouse using the piggyBac (PB) transposon system, consist of HA-tagged dCas9 fused with 10xGCN4. This system associated with p65-HSF1 and EGFP in tandem via P2A and T2A, respectively. The transgene is directed by the ubiquitous CAG promoter and is prevent by the *loxP*-stop-*loxP* (LSL) cassette to restore Cas9 expression inducible by Cre recombinase shown in **figure 9** [115].

2. MATERIALS AND METHODS

2.1.Animal Breeding Strategy

All experiments conducted on animals were approved by Acıbadem Mehmet Ali Aydınlar University Animal Experiment Local Ethics Committees with ACU-HADYEK 2023/42 code. Animal experiments were arranged according to the Association for Research in Vision and Ophthalmology's statement on the use of animals in research. Animals were located in Acıbadem University. Pyrat Animal Facility Software (https://www.scionics.com/pyrat.html) was used for storing animal maintenance records. All mice were kept on a 12-hour light/dark cycle with ad libitum food and water.

2.2. Breeding Strategy of dCas9-SPH Transgenic Mouse

dCas9-SPH transgenic animals with stock no 031645 were purchased from Jackson Laboratories. The dCas9-SPH inducible system allows simultaneous overexpression of multiple genes in SPH mice through the Cre recombinase system [115]. When these animals use single or multiple gRNAs and Cre protein together, they can adjust the dosage of mRNA synthesized from genes and can be used in *in vivo* cell programming for various diseases. dCas9-SPH transgenic mouse under the control of CAG promoter enables inducible expression of nuclease-deactivated dCas9, EGFP and SPH activator after it is activated by Cre recombinase.

These animals were obtained from Jackson laboratories in heterozygote form, and breed with C57BL/6 mice in the f1 generation to expand the animal numbers. F2 generation showed two different genotypes, dCas9-SPH$^{ki/wt}$ and dCas9-SPH$^{wt/wt}$. Afterwards dCas9-SPH$^{ki/wt}$ animals were breeded with each other. Finally, in the f3 generation showed three different genotypes dCas9-SPH$^{ki/ki}$, dCas9-SPH$^{ki/wt}$ and dCas9-SPH$^{wt/wt}$ **(Fig. 5).**

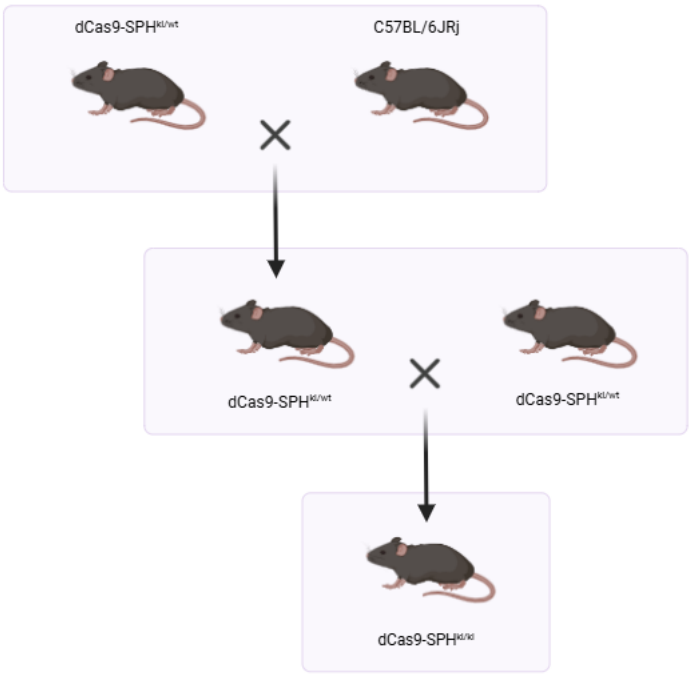

Figure 5. Breeding strategy for dCas9-SPH transgenic mouse line. *dCas9-SPH$^{ki/wt}$ animals which are bought from Jackson Laboratories are crossed with C57BL/6JRj mouse from our lab (F1). After crossing dCas9-SPH$^{ki/wt}$ animals with each other in the F2 generation, we obtained dCas9-SPH$^{ki/ki}$ animals in the F3 generation.*

2.3. Generation of Pou4f1$^{AP/AP}$ Transgenic Mouse

B6.Pou4f2(Ap)Kln/J transgenic mouse line also called *Pou4f2$^{Ap/Ap}$* is generated by Dr. William H. Klein`s and his colleagues [116].The Pou4f2-AP knock in allele has been generated by inserting an targeting cassette into *Pou4f2* locus containing an alkaline phosphatase gene. *Pou4f2* promoter/enhancer elements directs alkaline phosphatase expression. This insertion resulted in deletion of *Pou4f2* which resulted in severe loss of RGCs developmentally. This transgenic mouse line is used as a control showing the loss of RGC by ddPCR in our studies.

2.4. Genotyping

2.4.1 Toe Biopsy

For isolating DNA from transgenic mouse tissue toe biopsy was performed between postnatal day (PND) 5 to 8. Lysis buffer (50 µL) was added to collected tissue. Then tissues were incubated for 90 minutes at 95°C. After incubation tissues were neutralized by adding neutralization buffer (50 µL). Final samples were stored at -20°C.

Components	Volume (µL)	Final Concentration
Sodium Hydroxide	62,5	25 mM
EDTA	10	0,2 µM
Water	Up to 25 ml	

Table 1. Lysis buffer. *Components of lysis buffer and their concentrations*

Components	Volume (ml)	Final Concentration
Tris-HCl	1	40 mM
Water	24	

Table 2. Neutralization buffer. *Components of tissue neutralization buffer and their concentrations*

2.4.2 PCR Genotyping

2.4.2.1 dCas9-SPH PCR

For the construction of a common PCR master mix, GoTaq green PCR reaction buffer (Promega, M7911) was used.

Components	Volume (µl)	Final Concentration
GoTaq Green Reaction	1	1X
Buffer	1	1X
$MgCl_2$	0,3	2 mM
DMSO	0,2	1/21 (v/v)
dNTP	0,2	0,12 mM
Water	2,5	

Table 3. GoTaq Green Master Mix. *Preparation of GoTaq Green master mix.*

For standard PCR reactions Taq DNA polymerase (NEB, M0267L) was used. Toe biopsy tissues were used for performing PCR genotyping. 2 µl of sample from toe biopsy was added to each PCR reaction. All the components of PCR reaction mixture were added into a 0,2ml PCR tube (Sarstedt, 72.737.002) to be vortexed and spun. PCR tubes were placed in a thermal cycler (Biorad, C1000 Touch Thermal Cycler) and an appropriate PCR protocol was used from **tables 5 and 6.**

Components	Volume (µl)	Final Concentration
GoTaq Green Master Mix	21	
Taq Polymerase	0,15	0,06 U/µl

Forward Primer	1	50nM
Reverse Primer	1	50nM
DNA	1-2	
Nuclease Free Water	Fill up to 25	

Table 4. Standard PCR reaction. *Preparation of the standard PCR reaction structure.*

Steps	**Temperature**	**Time**
1	94°C	5 minutes
2	94°C	30 seconds
3	60°C	30 seconds
4	72°C	1 minute
5		Go to step 2 for 35 times
6	72°C	1 minute
7	4°C	hold

Table 5. dCas9-SPH Touchdown PCR Amplification. *Time intervals, temperate and cycle repeats for dCas9-SPH genotyping PCR reaction are shown.*

Agarose gel electrophoresis was performed after PCR

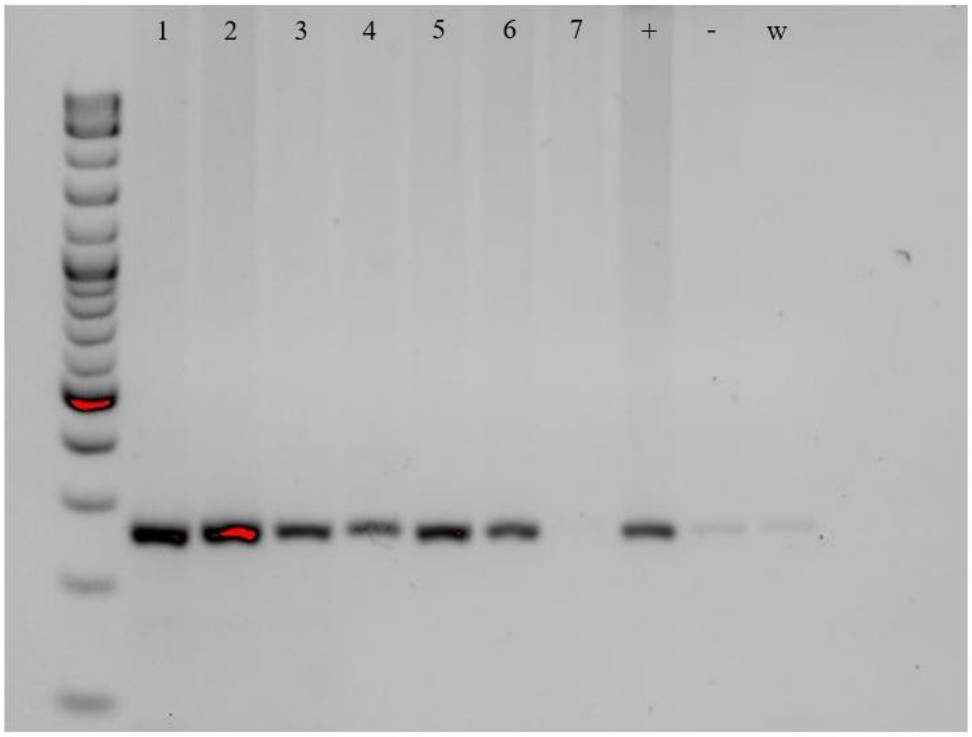

Figure 6. Representative Gel Image of dCas9-SPH PCR with Suntag primers. *Gel image shows that except the seventh sample, all samples are dCas9-SPH positive regarding to 264 bp transgene band with using dcas9-vp64 EGFP R (SunTag) and dcas9-vp64 HSF F (Sun Tag) primers. As a negative control which does not include transgene, C57BL/6 Control mouse was used. GENESTA 100 bp ladder was used.*

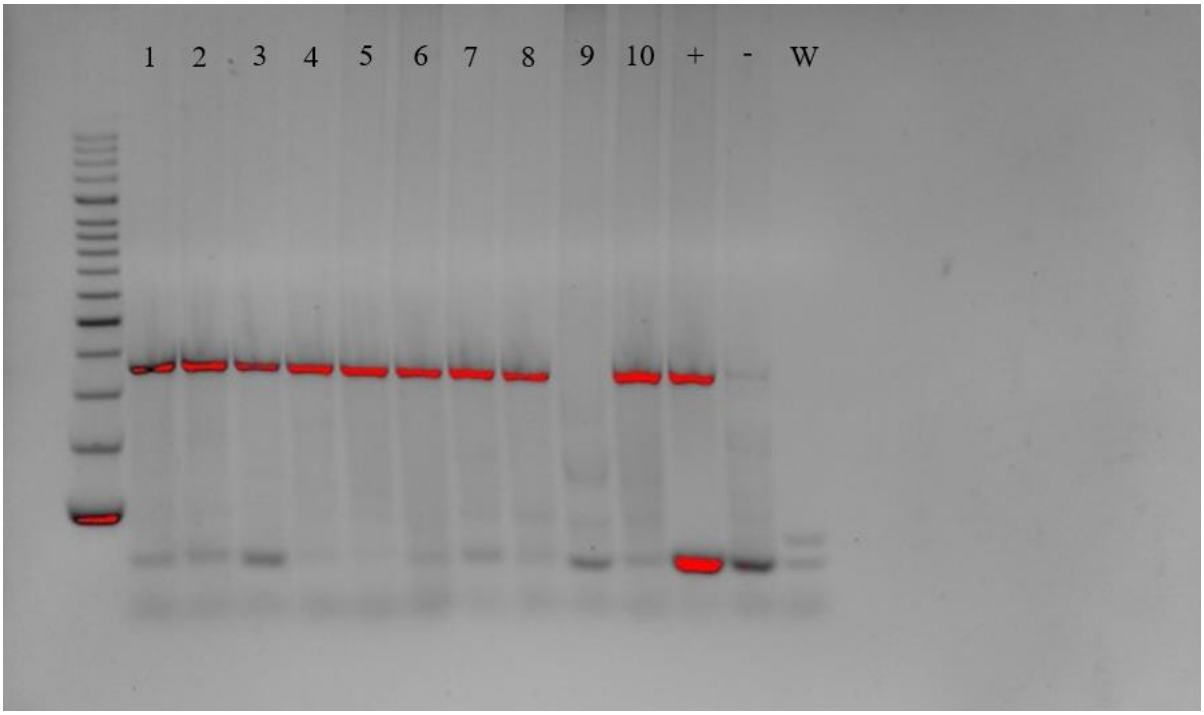

Figure 7. Representative Gel Image of dCas9-SPH PCR with wild-type primers. *Gel image shows that except the ninth sample, all samples have dCas9-SPH wild type genes, regarding to 324 bp transgene band with using SPH Common Forward and SPH Wild Type Reverse. As a negative control which includes the transgene, dCas9-SPH$^{ki/ki}$ control mouse was used. GENESTA 100 bp ladder was used.*

2.4.2.2 Pou4f2 PCR

Steps	**Temperature**	**Time**	**Note**
1	94°C	5 min	Denaturation
2	94°C	50 sec	Denaturation
3	68°C	1 min	Annealing
4	72°C	30 sec	Synthesis

5			Go back to step 2 for 8 times
6	94°C	50 sec	Denaturation
7	63°C	1 min	Annealing
8	72°C	30 sec	Synthesis
9			Go back to step 6 for 31 times
10	72°C	5 min	Elongation
11	10°C	Hold	Cool Down

Table 6. Pou4f2 AP PCR Amplification. *Time intervals, temperate and cycle repeats for Pou4f2 AP genotyping PCR reaction are shown.*

Agarose gel electrophoresis was performed after PCR

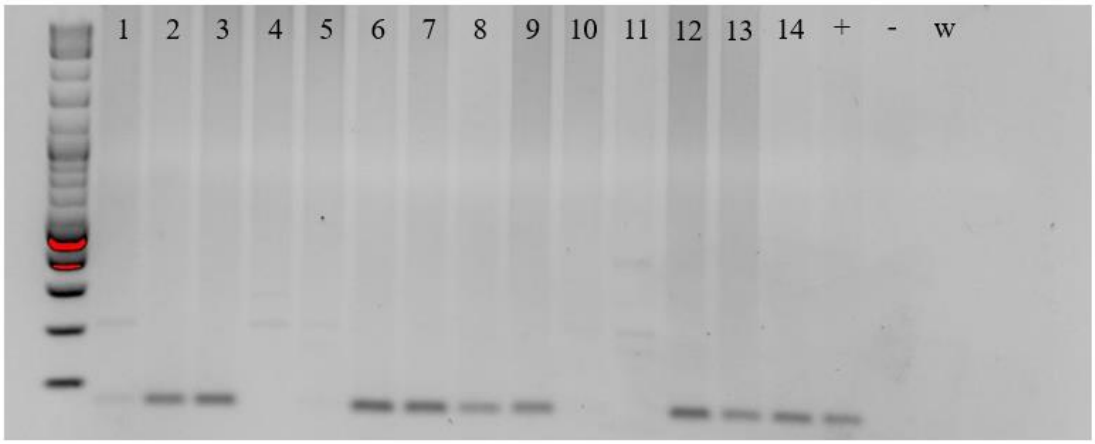

Figure 8. Representative Gel Image of Pou4f2 PCR with AP primers. *Gel image shows that second, third, sixth, seventh, eighth, ninth twelfth, thirteenth and fourteenth samples are Pou4f2-AP positive regarding to 95 bp transgene band. As a negative control which does not include transgene, C57BL/6 Control mouse was used. GENESTA 100 bp ladder was used.*

Primer Name	**Sequence**
Mus musculus dcas9-vp64 EGFP R (SunTag)	CTG AAC TTG TGG CCG TTT AC
Mus musculus dcas9-vp64 HSF F (Sun Tag)	CAC CAT CTC CCT GCT GAC A
Mus musculus SPH Mutant Reverse	TTATGTAACGCGGAACTCCA
Mus musculus SPH Common Forward	AGACAGGGGACTGGACAGAA
Mus musculus Pou4f2 Wild-Type Forward	CAAGCAGCTGAGCCCAAATC
Mus musculus Pou4f2 Wild-Type Reverse	ACAGTCAGCTCCTCGCTTTG

Table 7. List of Primers For PCR Genotyping of dCas9-SPH and Pouf2 animals*. PCR primers were designed by Primer BLAST software.*

2.4.3 Agarose Gel electrophoresis

50X TAE stock solution was prepared with 100 mL 500 mM EDTA (Merck, Cat#60004), 57.1 mL glacial acetic acid (Merck, Cat#64197) and 242 g Tris-base (Merck, Cat#77861), and filling up to 1L with ddH2O were used to prepare. 1X TAE solution and decent amount of agarose (GeneON BioScience, Cat Cat#604001) used to prepare agarose gel. Samples including positive, negative

and water controls for PCR genotyping were loaded into 2% (w/v) agarose-TAE gel, and run for 1 hour at 100V.

2.5.Retina Isolation

2.5.1 Whole Retina Isolation and Total RNA Isolation from Retina

Mice were sacrificed by using CO_2. The corneas of the mice were sliced open with a scalpel. With squeezing the eyecup using a forceps, lens and vitreous were removed. Afterwards, whole retina was isolated with a forceps and transferred into a 1,5 ml Eppendorf tube. The isolated retinas were stored at -80°C for further use.

For the isolation of the taken retinas, Roche High Pure RNA Isolation kit no:1182865001 was used. 400 µL Lysis/Binding-Buffer was added to retinas. The retinas were homogenized with a 1 ml syringe and 21 G needle with 8 to 10 strokes. 190 µL 100% EtOH was added and mixed well without vortexing. Lysate transferred to the Roche Spin Column. Mix was centrifuged 1 minute at full speed. Flow through was discarded and the column was putted back in same collection tube. The sample was incubated for 15 minutes at room temperature. 500 µL Wash Buffer I was added to the column. Mix was centrifuged 1 minute at full speed. Flow through was discarded and the column was putted back in same collection tube. 200 µL Wash Buffer II was added to the column. Mix was centrifuged 1 minute at full speed. Flow through was discarded and the column was putted back in same collection tube. Mix was centrifuged 1 minute at full speed for avoiding any Wash Buffer carryover. Flow through was discarded and the column was put in fresh 1.5 ml Eppendorf tube. 50 µL water was added directly on membrane without any contact. The sample

was incubated for 1 minute at room temperature. Column was centrifuged 1 minute at 10'000 rpm. The column was discarded and the isolated RNA was put directly on ice.

2.5.2 Whole Retina Isolation and Dissociation

For the whole retina isolation and dissociation a collection of materials and solutions were prepared. 1M HEPES was diluted to a concentration of 100Mm in HBSS. A 25mM l-cysteine solution was prepared by dissolving 30,3 mg l-cysteine in 10 ml DNase/RNase-free sterile water. 25Mm l-cysteine was aliquoted 100 µl each into microcentrifuge tubes and stored at -20 °C until further use. 5mM EDTA mix was made by dissolving 73 mg of EDTA in 50 ml DNase/RNase-free sterile water. The dissociation mixture was prepared fresh for each retina to be dissociated. Dissociation mixture was prepared by 40 µl papain (10108014001,Roche), 20 µl 5 mM EDTA, 20 µl 25 mM l-cystein and 320 µl 100 mM HEPES. Dissociation mixture was incubated for 15 minutes at 37°C. If the mixture prepared in bulk, it was distributed into microcentrifuge tubes. 3 ml of colorless DMEM mixture (31053028, Gibco) was prepared for each retina. DMEM mixture is prepared by 2%FBS,0,025% kolliphor-P188, and 0,1%Draq7 (424001,Biolegend). Tips of glass pPasteur pipettes (3233050, Marienfeld) were polished by heat.

Mice were sacrificed by using CO_2. The corneas of the mice were sliced open with a scalpel. With squeezing the eyecup using a forceps, lens and vitreous were removed. Afterwards, whole retina was isolated with a forceps and transferred into a 1,5 ml microcentrifuge tube containing dissociation mixture. Tubes were incubated for 7 minutes at 37°C. 1 ml of colorless DMEM mixture was added after the dissociation mixture was discarded. The whole retinas were dissociated with flowing the mixture up and down by using a glass Pasteur pipettes with a rubber suction ball. Dissociated retinas were filtered through a 70 µm cell strainer (pluriStrainer, 431007060, Pluriselect) into a 5 ml round bottom tube (352235, Falcon). 2 ml of colorless DMEM

mixture was added through the 70 μm cell strainer into the tube. The tube was placed on ice. After dissociation Flow Cytometry analysis was performed.

2.6. NanoDrop Analysis

Isolated RNAs were taken to Nanodrop to measure their concentration. NanoDrop setting were adjusted to measure RNA samples. 1 μl water (the same water that has been used in the RNA Isolation) was uploaded on the sample testing area as blank. After measuring the blank 1 μl of samples was uploaded on the sample testing area for measuring their concentrations.

2.7. Assessment of gRNAs in vitro

2.7.1 cDNA Synthesis

cDNA is the first step for the gene expression analysis protocols. High-Capacity cDNA Reverse Transcription kit no:4368814 was used. The procedure for one sample is 5 μL Random Primer, 5 μL RT Buffer, 2 μL dNTP Mix and 1.25 μL Reverse Transcriptase Multiscribe Enzyme with a total of 13.25 μL. Sample amount is calculated by using concentrations of RNAs. The protocol requires 500 ng of sample. After calculating the required μL for 500 ng sample. Water was added to the mixture to make a total of 50 μL mixture for one reaction. After preparing the mixture the samples were uploaded to the thermocycler. The samples were stored at -20°C.

Regaents	**Volume**	**Concentration**
Random Primer	5 µL	10X
RT Buffer	5 µL	10X
dNTP Mix	2 µL	100mM
Reverse Transcriptase Multiscribe Enzyme	1,25 µL	20 U/ µL
Water	Fill up to 50 µL	
Sample	500 ng (X µL)	

Table 8. Standard cDNA Synthesis. *Preparation of the standard cDNA synthesis.*

1	25°C	10 min
2	37°C	90 min
3	85°C	5 min
4	4°C	hold

Table 9. Reverse transcription protocol. *Protocol for the reverse transcription of cDNA.*

2.7.2 Digital Droplet PCR (ddPCR)

cDNAs were diluted using Rnase/Dnase free water at ratios of 1:40 for *Gapdh* and *Rho*; 1:10 for *Nfl*, *Opn4* and *Pou4f1*. *Gapdh* and *Rho* were diluted as 1:40 because of their increased expression compared to *Nfl*, *Opn4* and *Pou4f1.* For each primer test 1 µL (10 ng) of the diluted retina cDNAs

were used. A 20 µL PCR reaction mix including 1 µL of cDNA that has been diluted 1:40 and 1:10, 125 nM primers, and 2x evagreen super mix was used to create droplets. The center of the cartridge was loaded with sample mix to create droplets. Samples were put into a cartridge, and the bottom row of the cartridge was then filled with 70 µL of the droplet generation oil. The cartridge was inserted into the droplet generator with a gasket on top. It is essential to ensure in this section that no gaps exist between the gasket and the cartridge at this stage. Once the droplets formed, they were carefully removed from the top rows in amounts of around 40 µL and immediately transferred to the semi-skirted 96-well PCR reaction plate. Semi-skirted PCR plate was sealed with aluminum foil using a PCR plate sealer. PCR plate was then located to the 96-well heat-sealed thermal cycler. The PCR protocol was performed with the following conditions: 95 °C for 5 minutes, 95°C for 30 seconds for 40 cycles, 60°C for 1 minute, 4 °C for 5 minutes, 90 °C for 5 minutes and 4 °C infinite hold PCR protocol was run. A ramp rate of 2 °C/s was applied during each cycle for PCR amplification to achieve the appropriate temperature for each step during the amplification in order to preserve the droplet integrity.

Primer Name	**Sequence**
Mus musculus Pou4f1 Forward	CCTCGTCTGAGAAGATCGCC
Mus musculus Pou4f1 Reverse	CGGTTCTCCAAAGGAGGGAG
Mus musculus NFL-1 Forward	CAAGGACGAGGTGTCGGAAA
Mus musculus NFL-1 Reverse	TGATTGTGTCCTGCATGGCG
Mus musculus Melanopsin Forward	CCAGCTTCACAACCAGTCCT
Mus musculus Melanopsin Reverse	CAGCCTGATGTGCAGATGTC
Mus musculus Rhodopsin Forward	CTTCACCTGGATCATGGCGTT
Mus musculus Rhodopsin Reverse	TCGTTGTTGACCTCAGGCTT

Mus musculus Dpysl2 Forward ex13-14	CAGCTAAGACATCCCCTGCC
Mus musculus Dpysl2 Reverse ex13-14	TCGTCAATCTGAGCACCAGAC
Mus musculus Dpysl2 Forward ex12-13	ACGGCACACTTCATGTCACT
Mus musculus Dpysl2 Reverse ex12-13	CGTCACAGACACCTCGCATA
Mus musculus Dpysl2 Forward ex 4-6	CGGGGTAAACTCCTTCCTCG
Mus musculus Dpysl2 Reverse ex 4-6	GACTTGAGCTATGGCACCGA
Mus musculus Dpysl2 Forward ex11-12	CCAAGACACACAACAGTGCTC
Mus musculus Dpysl2 Reverse ex11-12	AGCCTGCTCCTTGCTTTGAT
Mus musculus Dpysl2 Forward ex 3-4 II	CGGAGGGATTGACGTGCATA
Mus musculus Dpysl2 Reverse ex 3-4 II	CCACTGATCAAAGGCAGCCA
Mus musculus GAPDH ddPCR Forward	CAGCAATGCATCCTGCACC
Mus musculus GAPDH ddPCR Reverse	TGGACTGTGGTCATGAGCCC

Table 10. List of Primers For ddPCR Gene Expression Analysis of Pou4f1, Melanopsin, NfL, Rho Dpysl2 and Gapdh gene analysis. *ddPCR primers were designed by Primer BLAST software*

2.8.*In vivo* Imaging Techniques

2.8.1 MicronIV Retina Fundus and Fluorescence Imaging

For Retinal imaging MicronIV from Phoenix Instruments was used for the fluorescence and fundus imaging of common reporter molecules including Green Fluorescent Protein (GFP), Yellow Fluorescent Protein (YFP) and monomeric Cherry (mCherry) and also fundus images. Two different drops were applied into each mouse eye to enlarge the pupil, tropicamide (0.5%) and

phenylephrine hydrochloride (2.5%). After the pupils were enlarged, mouse is located to the imaging stage for anesthesia. Anesthesia was performed with a mouthpiece on the imaging stage. The initial induction of anesthesia is started with 5% isoflurane (1L/min) to implement deep anesthesia of mice. After that 1.5% isoflurane (1L/min) is used to keep the mice sedated. We have checked key indicators for confirming deep anesthesia such as the tail pinch reaction, loss of righting reflex and the withdrawal reflex. 0.2% carbomer 980 topical gel was applied to the mouse eye to prevent the surface of the eyes from drying out under anesthesia. As a coupling gel for imaging after the mouse was placed on the imaging platform. Proper pupil dilation was assured. MicronIVs nosepiece and imaging stage were adjusted to align with each other. Once the eye is in its proper position in the center, objective was moved gently until it makes contact with the pupil.

Early genotyping in dCas9-SPH mouse models can provide critical, first-hand insights during the weaning stage.

For dCas9-SPH mouse models, the detection / leakage of GFP expression indicates SPH expression; however, this does not confirm that the mouse is homozygous dCas9-SPH. Conversely, the absence of GFP expression suggests the mouse is of the wild-type genotype.

Additionally, if GFP expression is observed alongside a dark circle around the optic nerve—most visible under a brightfield lens—it most likely indicates optic cupping. This phenotype strongly correlates with the genotype dCas9-SPH $^{ki/ki}$.

2.8.2 Optical Coherence Tomography (OCT)

Optical Coherence Tomography (OCT) which is known as an effective non-invasive imaging method was used to image the retina at micron scales in cross sections with high definition. This technique is used to measure and observe the retinal layers to evaluate the changes regarding retinal thickness. For in vivo imaging our laboratory used OcuScience OCT system. Mice were anesthetized and prepared for imaging with the same procedure mentioned above ***(2.8.1)*** for the imaging procedure of OCT. When the mice located properly on the imaging stage and optic nerve monitored on the computer, scanning of the retina was started. Then, the average of the scan data is taken and used for retinal layer assessments.

Optical Coherence Tomography (OCT) shows the cross sections of the retina. It is mostly used for observing the layers of the retina clearly. However, in our case it is also helpful for genotyping. The layers are mostly linear to each other in most cases, but we saw a different formation while we are observing dCas9-SPH$^{ki/ki}$ mice. dCas9-SPH$^{ki/ki}$ mice retina forms a cupping between the layers called Optic Cupping, which was very helpful for the genotyping part.

2.9.pAAV-sgRNA Vector Design

As a backbone pAAV-Cre (pAAV.CMV.HI.eGFP-Cre.WPRE.SV40, Addgene#105545) AAV vector was used. Primers that had restriction enzyme insertions were generated to clone 423 bp region containing gRNA, sgRNAs and U6 promoter scaffold into this vector. Reverse primers target the gRNA scaffold downstream. On the other hand forward primers target the U6 promoter upstream. Insertions made to the 5' end forward and reverse primers were targeted by multiple restriction enzymes to enable further modifications of produced vectors.

3. RESULTS

3.1 Analysis of Retinal Integrity and GFP Leakage Across Genotypes

We obtained dCas9-SPH transgenic mice from Jackson Laboratories for gene regulatory studies. The heterozygous transgenic mice (dCas9-SPH$^{ki/wt}$) were bred with C57BL/6 animals. During this process, we observed unexpected abnormalities, including GFP leakage. Notably, GFP expression was not anticipated due to the presence of the Cre-Lox recombination system, which includes an LSL (Lox-Stop-Lox) cassette that introduces an early stop codon to prevent translation (**Fig. 9**). Despite the system being in a closed state, translation was unexpectedly active. Our thoughts for the GFP expression are, it might be occurring due to the T2A ribosome-skipping sequence (**Fig. 10E & H and Fig 11**). The downstream P2A sequence, despite containing a premature termination codon (PTC), appeared to escape the typical nonsense-mediated mRNA decay (NMD) and engage in translation, potentially producing a truncated protein under these conditions. We hypothesize that transcripts are still available despite the LSL cassette which might be enabling. P2A functionality, resulting in GFP protein translation and leakage shown in **figure 10E & H**. This leakage was also confirmed by the flow cytometry of the dissociated retina compared to naïve control retinas (**Fig 11A &B**). Transduction of AAVs vectors that express EGFP and Cre further increased the EGFP levels (**Fig. 11C**).

Following the observation of GFP leakage as unanticipated, we proceeded to analyze and compare fundus and OCT images. Fundus brightfield and fluorescent images, along with OCT images, were examined across three different genotypes. We first observed dCas9-SPH$^{ki/wt}$ animals and they displayed GFP leakage in fluorescent images, although the retina layers appeared intact and

healthy in OCT images **(Fig. 10C-F)**. After breeding the dCas9-SPH$^{ki/wt}$ animals with C57BL/6 animals we examine the f2 generation which are dCas9-SPH$^{ki/wt}$ animals and wild-type animals which will be referred as dCas9-SPH$^{wt/wt}$ animals. As expected, dCas9-SPH$^{wt/wt}$ animals exhibited no GFP leakage in fluorescent images and demonstrated a structurally normal retina in OCT images **(Fig. 10A-C)**. In the f3 generation dCas9-SPH$^{ki/ki}$ animals began to emerge. These dCas9-SPH$^{ki/ki}$ animals, which occasionally exhibited phenotypic abnormalities such as infantilism, showed GFP leakage as well as a dark circular region around the optic nerve in both brightfield and fluorescent fundus images, accompanied by a near-collapse of the retinal layers in OCT images **(Fig. 10 G-I)**. Therefore, we examine the dCas9-SPH$^{ki/ki}$ animals more carefully and we found that the dark circle around the optic nerve compared the collapsed OCT images showed that this deformity is called optic cupping. After careful evaluation, we hypothesized that this optic cupping model could be correlated to a late stage of glaucoma.

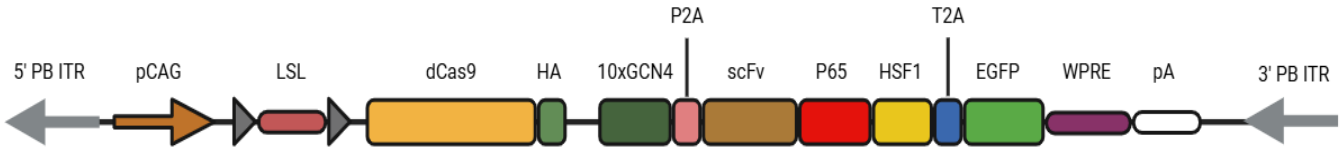

Figure 9. Cre-dependent SPH transgenic mouse. *Schematic representation of the Cre-dependent SPH vector used for generating transgenic mice with the piggyBac transposon. Figure adapted from https://www.nature.com/articles/s41593-017-0060-6, generated using https://app.biorender.com/*

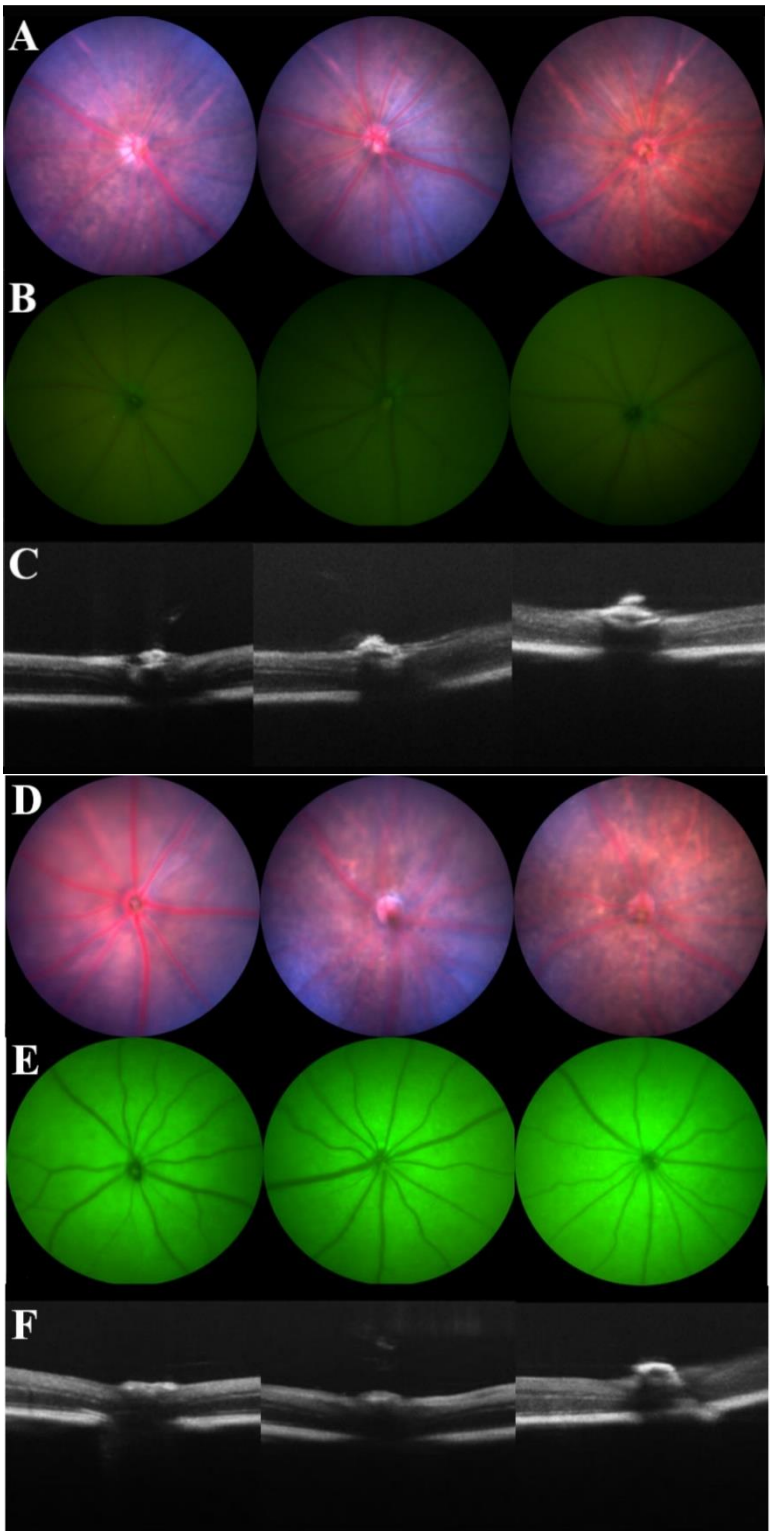
A
B
C
D
E
F

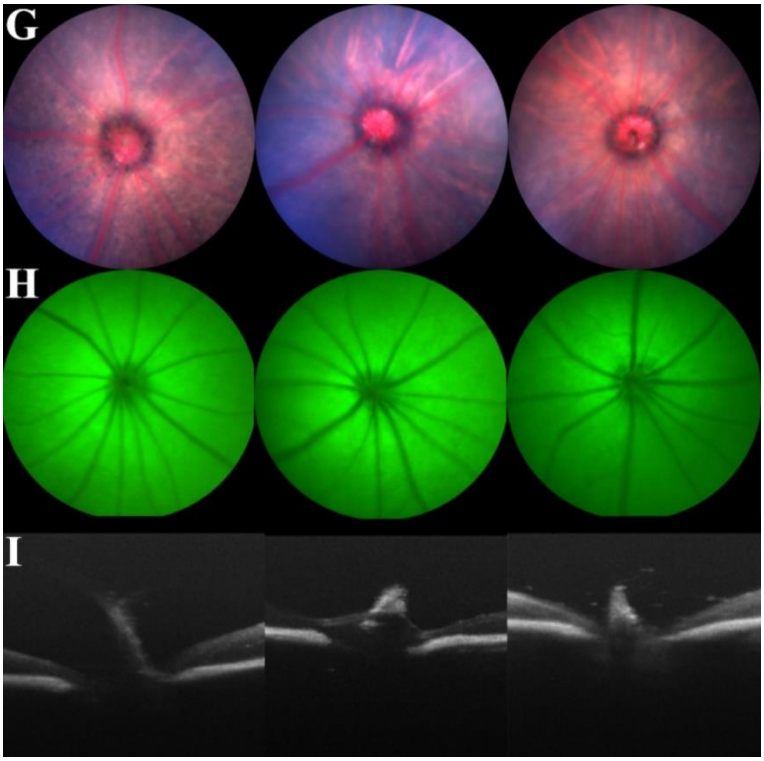

Figure 10. Fundus and OCT features of dCas9-SPH mice. A) *Fundus bright field images from three dCas9-SPH$^{wt/wt}$ animals.* ***B)*** *Fundus fluorescent image from three dCas9-SPH$^{wt/wt}$ animals which does not show any GFP expression or a dark circle around the optic nerve.* ***C)*** *Healthy OCT images from three dCas9-SPH$^{wt/wt}$ animals.* ***D)*** *Fundus bright field images from three dCas9-SPH$^{ki/wt}$ animals.* ***E)*** *A leaky GFP expression but no dark circle can be observed in high exposure settings in fundus fluorescent image from three dCas9-SPH$^{ki/wt}$ animals.* ***F)*** *Healthy OCT images from three dCas9-SPH$^{ki/wt}$ animals.* ***G)*** *Fundus bright field images from three dCas9-SPH$^{ki/ki}$ animals which shows a dark circle around the optic nerve.* ***H)*** *A dark circle around the optic nerve and a leaky GFP expression can be observed in high exposure settings in fundus fluorescent image from three dCas9-SPH$^{ki/ki}$ animals.* ***I)*** *OCT images from dCas9-SPH$^{ki/ki}$ animals shows an abnormaly in the optic nerve*

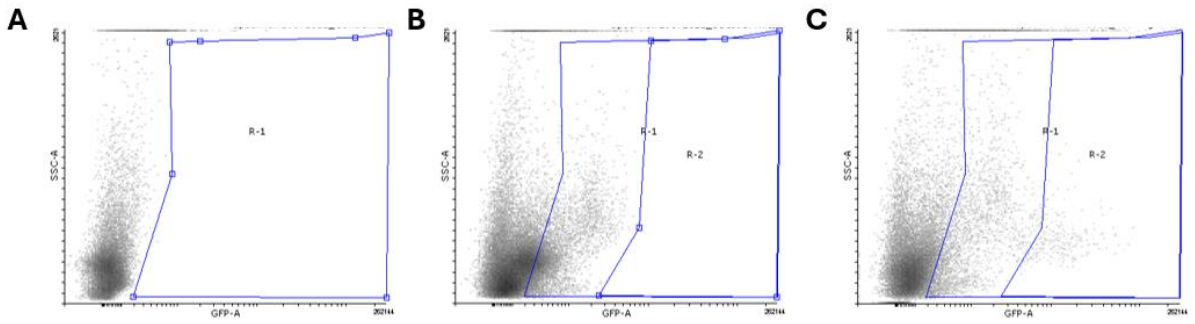

Figure 11. Flow cytometry analysis of dCas9-SPH retinas. *Flow cytometry analysis of wild type* ***A)*** *dCas9-SPH* ***B)*** *and AAV-GFP-Cre injected dCas9-SPH retinas* ***C)*** *Both AAV injected* ***C)*** *and uninjected* ***B)*** *dCas9-SPH retinas showed %19.9 GFP positive cells (R1 population) compared to %0.05 in wild type retinas. AAV injected dCas9-SPH retinas* ***C)*** *also showed highly increased GFP levels (R2 population, %3.3) due to GFP expression from AAV vector. Flow cytometry analysis was performed by using Flowing Software 5.2*

3.2 Intraocular Pressure Assessment Across Genotypes

Several studies have established that elevated intraocular pressure (IOP) is a key pathophysiological factor in glaucoma [117]. Based on these findings, we hypothesized that our homozygous model might mimic glaucoma and have an increased IOP, prompting us to assess IOP levels across three different genotypes. A total of nineteen animals were examined, comprising five dCas9-SPH$^{ki/ki}$, eight dCas9-SPH$^{ki/wt}$, and six dCas9-SPH$^{wt/wt}$ subjects. IOP measurements were conducted. The averages for three genotypes are, 17,58 mm Hg for dCas9-SPH$^{wt/wt}$ animals, 17,66 mm Hg for dCas9-SPH$^{ki/wt}$ animals and 18,06 mm Hg for dCas9-SPH$^{ki/ki}$ animals. Despite the optic cupping phenotype, our findings do not reveal any differences in IOP among the three genotypes **(Fig. 12)**. This suggested that optic cupping phenotype may be a result of genetic mutations that directly affects optic nerve development or function without elevated intraocular

pressure (IOP) which may serve as a novel hereditary optic neuropathy model. For the analysis of the results ordinary one-way ANOVA test was used. From multiple comparisons, Dunnett's multiple comparison test was chosen and dCas9-SPH$^{wt/wt}$ was used as a control.

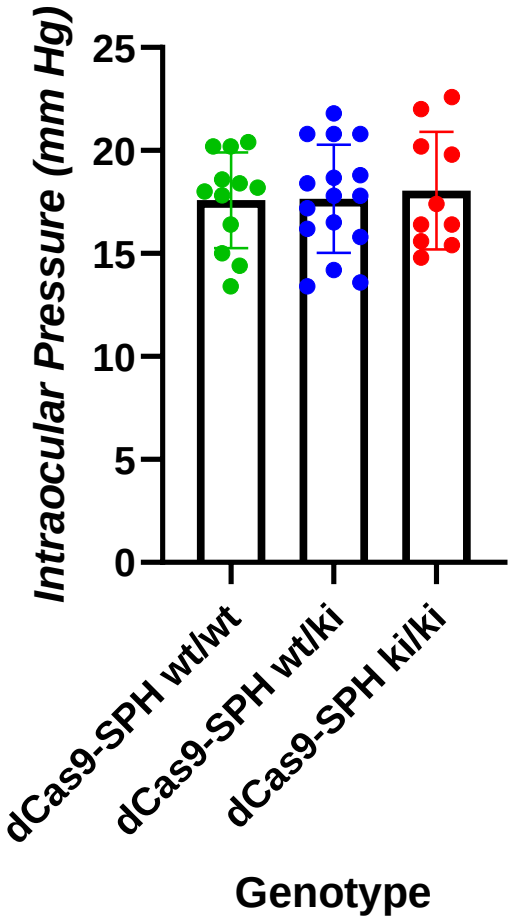

Figure 12. IOP measurements from three different genotypes. *Transgenic mouses IOP's from all three different genotypes were measured at six to eight weeks. The collected data showed no significant difference between three genotypes. One-way ANOVA with Dunnett's post-tests was used to compare control levels (dCas9-SPH$^{wt/wt}$) with expression levels of each genotype (ki/wt, ki/ki).*

3.3 ddPCR-Based Analysis of Retinal and Neurodegenerative Gene Expression

Since there is no IOP change between three genotypes, we have to know if there is an RGCs loss or not in this phenotype since it is another symptom of glaucoma. To investigate whether dCas9-SPH$^{ki/ki}$ animals have an RGC loss, we analyzed the expression levels of four retinal genes—*Pou4f1*, *Opn4*, *Nfl*, and *Rho* —relative to the housekeeping gene *Gapdh* using ddPCR from cDNA samples made from RNAs made from RNA isolation of three different genotypes. *Gapdh* levels were measured in all three genotypes as a reference housekeeping gene. We then calculated the expression ratios of each of the four target genes to *Gapdh*.

These genes were chosen based on their relevance to glaucoma pathology (RGC survival) and neurodegenerative disorders. Glaucoma is characterized by the progressive loss of retinal ganglion cells (RGCs) and the retinal nerve fiber layer, leading us to first examine *Pou4f1*, a transcription factor critical for RGC development. *Pou4f1* encodes brain-specific homeobox/class IV POU-domain transcription factors, which regulate various stages of RGC development, including axon guidance, neuronal differentiation, synapse formation, migration, and dendrite development [118, 119]. This gene also shows the presence of the RGC cells as it is already expressed in the adult RGCs as well [120]. As it seen in **Fig. 13A** *Pou4f1* gene expression did not change between dCas9-SPH$^{ki/ki}$ and dCas9-SPH$^{wt/wt}$ genotypes, which means there is no significant RGC loss in dCas9-SPH$^{ki/ki}$ genotype.

Next, we assessed *Opn4*, the photopigment expressed in intrinsically photosensitive RGCs (ipRGCs) projecting to the suprachiasmatic nucleus. *Opn4* transcription levels show some

reduction but not significant. There was a decrease in the amount of *Opn4* in ipRGC in the Pou4f2 knockout retina which is consistent with the developmental RGC loss and was not previously analyzed according to our knowledge. It is important to note that the reduction of *Opn4* is not as severe as *Pou4f1* and *Nfl* suggesting that ipRGCs are not as significantly affected as the other RGC populations in the *Pou4f2* knockout retina **(Fig. 13B).**

To further explore neurodegenerative aspects, we analyzed *Nfl* gene expression levels, as NfL (a neurofilament subunit) is essential for maintaining neuronal structural stability, integrity, and impulse conduction [121]. There was no significant difference between three genotypes for NFL similar to POU4F1 which are key RGC markers which shows that there is no RGC death in all these three genotypes. The Pou4f2$^{AP/AP}$ model serves as a reliable tool for studying RGC development and survival. This is due to the critical role of Pou4f2 in RGC differentiation, with its absence leading to impaired differentiation and increased apoptosis of RGCs **(Fig. 13C)** [116]. Finally, we examined *Rho* for a broader retinal involvement, which is the gene encoding the rod photoreceptor visual pigment, as an additional marker of photoreceptor degeneration to see if the photoreceptors are already intact in this model [122]. *Rho* data analysis showed the most interesting finding, which is no photoreceptor change in any of these three genotypes. However surprisingly, although there are no issues with the photoreceptor layer integrity in the Pou4f2$^{AP/AP}$ mouse, there was a very significant reduction of rhodopsin which suggested the photoreceptors do not express rhodopsin despite they are alive **(Fig. 13D)**. This suggested there is no RGC or photoreceptor differences between any of the dCas9-SPH genotypes. Since there is a severe loss of RGCs in Pou4f2$^{AP/AP}$. the rhodopsin expression is most likely suppressed in Pou4f2 knockout retina which is a novel finding **(Fig. 13D).** For the analysis of the results ordinary one-way ANOVA

test was used. From multiple comparisons, Dunnett's multiple comparison test was chosen and dCas9-SPH$^{wt/wt}$ was used as a control **(Fig. 13).**

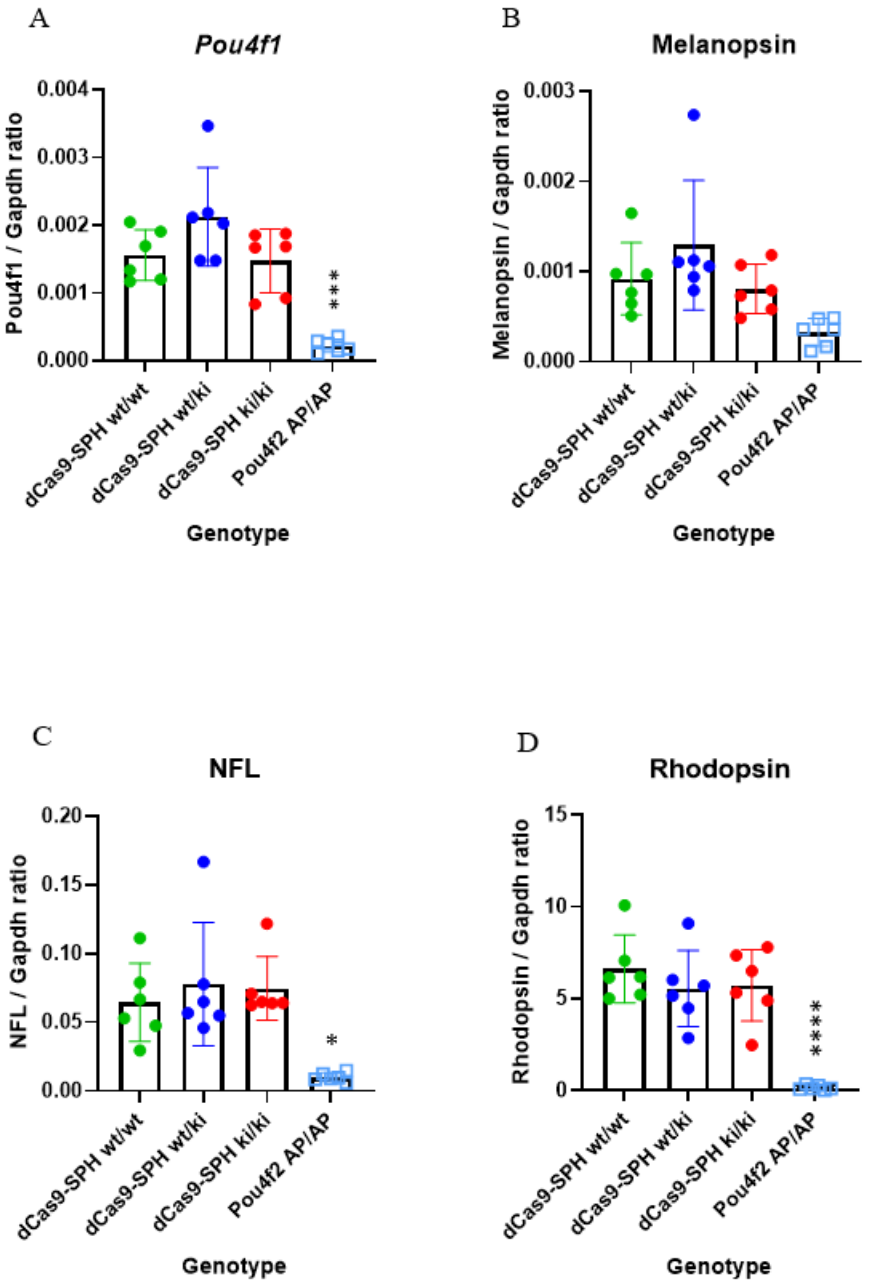

Figure 13. Primer testing for different genotypes. ***A)****Pou4f1,* ***B)****Opn4,* ***C)****Nfl and* ***D)****Rho genes were checked with ddPCR for four genotypes dCas9-SPH$^{ki/ki}$, dCas9-SPH$^{ki/wt}$, dCas9-SPH$^{wt/wt}$ and Pou4F2$^{AP/AP}$ and their ratios are taking with a housekeeping gene called Gapdh. Shown are means ± S.D. for N=6 per group. One-way ANOVA with Dunnett's post-tests was used to compare control levels (dCas9-SPH$^{wt/wt}$) with expression levels of each genotype (ki/wt, ki/ki, and Pou4f2$^{AP/AP}$). *P<0.05; **P<0.01; ***P<0.005; ****P<0.0001*

3.4 Genotypic Analysis of dCas9-SPH Variants and Correlation with Optic Cupping Phenotype

We wanted to check whether this phenotype is randomly occurring or there is an order that took place we wanted to see all the animals we have on hand. We check a total of 32 number of animals, out of these 32 animals we found 12 dCas9-SPH$^{ki/wt}$ animals, 10 dCas9-SPH$^{ki/ki}$ animals and 10 dCas9-SPH$^{wt/wt}$ animals. 12 dCas9-SPH$^{ki/wt}$ animals which has PCR data for the confirmation on the genotype. 12 of them has MicronIV and OCT images and they did not show any optic cupping phenotype. We check 10 of dCas9-SPH$^{ki/ki}$ animals with PCR genotyping. All 10 of them has MicronIV and OCT imaging and all showed optic cupping phenotype. We check 10 dCas9-SPH$^{wt/wt}$ animals that had PCR genotyping, 10 of them has MicronIV and OCT imaging and any of them did not show any optic cupping phenotype.

Genotype	***PCR confirmed***	***Cupping phenotype by MicronIV imaging***	***Cupping phenotype by OCT imaging***
dCas9-SPH$^{wt/wt}$	***10***	***0***	***0***

dCas9-SPH$^{ki/wt}$	***12***	***0***	***0***
dCas9-SPH$^{ki/ki}$	***10***	***10***	***10***

Table 11. Mouse genotypes checked with PCR, MicronIV and OCT

3.5 Integration of dCas9-SPH in Dpysl2 Gene and Its Potential Knockout Effect

We obtained this transgenic mouse model from Jackson Laboratories, which initially reported the integration of the construct at two loci, specifically on chromosomes 3 and 14 by Zhou et al [115]. However, the analysis of The Jackson laboratories and our analysis revealed that the integration is confined to chromosome 14, specifically within the *Dpysl2* gene. Given the substantial size of the dCas9-SPH sequence, 11.5 kb within the intronic region **(Fig. 9)**, we hypothesized that it might have disrupted the gene, potentially resulting in a knockdown effect. Since the dCas9-SPH has been inserted to the third intron of *Dpysl2* there is a high possibility that this might interfere the gene expression.

The Dihydropyrimidinase-like (*DPYSL*) proteins, also designated as the Collapsin response mediators (*CRMP*) proteins, mostly expressed in the development of the nervous system however, downregulated in the adult mouse brain [123-125]. Collapsin response mediator protein 2 (*Crmp2*) plays important roles in the formation of neural circuitry since it is a well conserved tubulin-binding cytosolic protein in model organisms such as rodents and zebrafish [126]. *Dpysl2* proteins mediate signals for various extracellular and intracellular pathways. Major roles of *Dpysl2* are numerous cellular processes such as neurite extension [127], dendritic spine development [128],

axonal guidance [129-132], synaptic plasticity [133] and cell migration [134]. The human *Dpysl2* gene has been implicated in a large variety of neurological disorders including neurodegenerative disorders such as Alzheimer disease [135], sensory and motor neuron disorders such as ALS [136], Batten disease [137], Huntington's disease [138] and central disorders such as epilepsy, bipolar disorder and schizophrenia [139-143]. *CRMP2* is also a susceptibility locus for schizophrenia [129, 144-146]

Dpysl2 gene is a neuronal gene mentioned above, therefore, there is a possibility dCas9-SPH insertion might also knock out the gene itself and the phenotype we observe might be related to this. So, we check whether this is the case. To investigate this possibility, we examined the transcriptional activity of *Dpysl2* genes by ddPCR and using different primer sets that target different regions of the transcript itself. **(Fig. 14).** The 'ex' in the name of the primers refers to exon. Our results showed a knockdown for the Dpysl2 gene in dCas9-SPH$^{ki/ki}$ animals and also a gradual reduction between the dCas9-SPH$^{wt/wt}$ animals, dCas9-SPH$^{ki/wt}$ animals and dCas9-SPH$^{ki/ki}$ animals, respectively. This suggested that the optic cupping phenotype we observed is most likely attributable to knockdown of the *Dpysl2* gene in dCas9-SPH$^{ki/ki}$. For the analysis of the results ordinary one-way ANOVA test was used. From multiple comparisons, Dunnett's multiple comparison test was chosen and dCas9-SPH$^{wt/wt}$ was used as a control. Test for Trend analysis is also done and showed a positive result for this gradual reduction

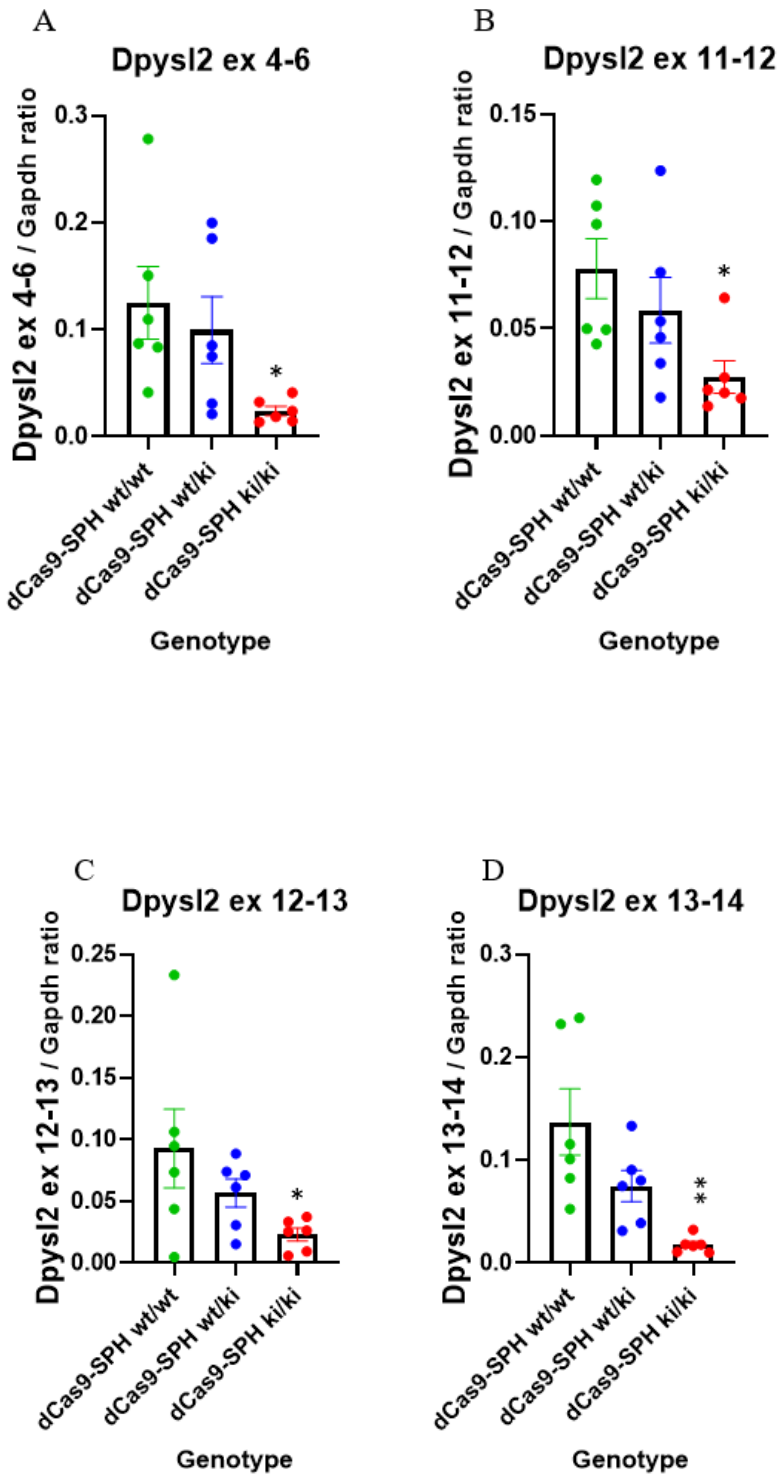
A
Dpysl2 ex 4-6
Dpysl2 ex 4-6 / Gapdh ratio
0.3
0.2
0.1
0.0
*
dCas9-SPH wt/wt
dCas9-SPH wt/ki
dCas9-SPH ki/ki
Genotype
B
Dpysl2 ex 11-12
Dpysl2 ex 11-12 / Gapdh ratio
0.15
0.10
0.05
0.00
*
dCas9-SPH wt/wt
dCas9-SPH wt/ki
dCas9-SPH ki/ki
Genotype
C
Dpysl2 ex 12-13
Dpysl2 ex 12-13 / Gapdh ratio
0.25
0.20
0.15
0.10
0.05
0.00
*
dCas9-SPH wt/wt
dCas9-SPH wt/ki
dCas9-SPH ki/ki
Genotype
D
Dpysl2 ex 13-14
Dpysl2 ex 13-14 / Gapdh ratio
0.3
0.2
0.1
0.0
**
dCas9-SPH wt/wt
dCas9-SPH wt/ki
dCas9-SPH ki/ki
Genotype

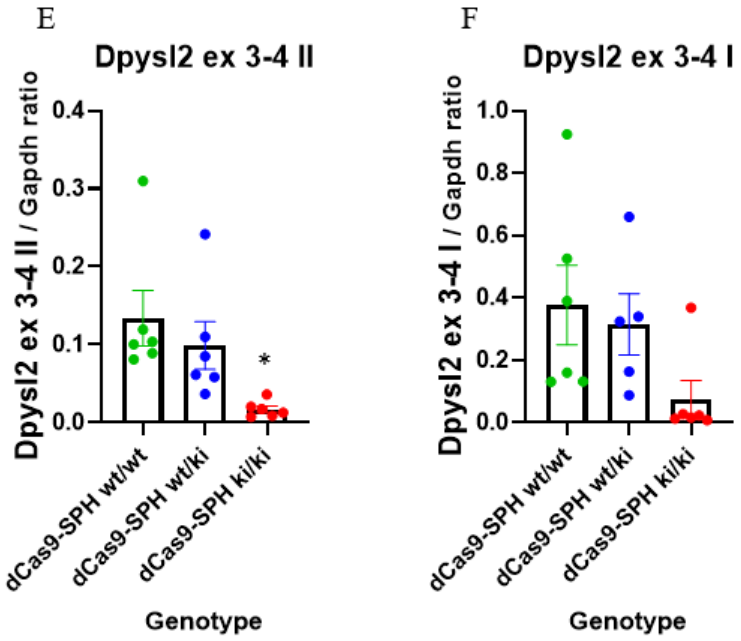

Figure 14. Primer testing for Dpysl2 gene between genotypes. *5 different primers* ***A)*** *Dpysl2 ex 4-6,* ***B)****Dpysl2 ex 11-12,* ***C)****Dpysl2 ex 13-14, ,* ***D)****Dpysl2 ex 12-13,* ***E)****Dpysl2 ex 3-4 II and* ***F)****Dpysl2 ex 3-4 I were checked for the expression of the Dpysl2 gene between dCas9-SPH$^{ki/ki}$, dCas9-SPH$^{ki/wt}$, dCas9-SPH$^{wt/wt}$ genotypes. Shown are means ± S.E.M. for N=6 for A, B, C, D and E groups; N=5 for F. One-way ANOVA with Dunnett's post-tests was used to compare control levels (dCas9-SPH$^{wt/wt}$) with expression levels of each genotype (ki/wt, ki/ki, and Pou4f2$^{AP/AP}$). *P<0.05; **P<0.01; ***P<0.005*

4. DISCUSSION

Glaucoma is an irreversible eye disorder with a range of different pathophysiology, prognoses, risk factors and treatments [31]. The increase in the IOP and loss of RGCs are the common risk factors of glaucoma [32]. Glaucoma is a multifactorial disease and some common types of

glaucoma are primary open-angle glaucoma (POAG), juvenile-onset open-angle glaucoma (JOAG), normal tension glaucoma (NTG) and primary congenital glaucoma (PCG). The extensively recognized feature of glaucoma is the enlargement of the cup the disc ratio, called optic nerve cupping. The dCas9-SPH animals which was obtained from Jackson Laboratories showed a dark circular shape around the optic nerve looked like optic cupping only in homozygous animals. The dCas9-SPH transgenic animals showed GFP leakage in both homozygous and the heterozygote animals

Leakage of GFP in dCas9-SPH$^{ki/ki}$ and dCas9-SPH$^{ki/wt}$ transgenic animals suggests that, SPH most likely leaks and translated due to P2A and T2A sequences. There may be some promotor like element or transcription start site bypassing the stop codon at the start of dCas9 in the gene construction. Since the P2A or T2A stops and restarts translation after releasing of the prelude protein, no effect on tract on GFP or SPH translation occurs. Since there is not any regulation on expression, SPH is expressed probably early on in embryonic stages. Early on, activator overexpression seems to be affecting the transcriptome profile by excess activation of these genes, since they are fusion *Hsf1* and the *p65*, we can anticipate an overexpression of these factors. Our initial thought of this phenotype was independent of an unspecific gene insertion knockout but most likely related to activator leakage similar to our observation on GFP expression leakage. Another reason might be even though the construct of the gene contains a premature stop codon, it is escaping the typical nonsense-mediated mRNA decay and continue in translation and LSL cassette cannot achieve complete repression of the downstream elements and GFP leaks. To confirm whether this observation was due to autofluorescence, we conducted an analysis using FACS flow cytometry. The results confirmed that the signal was not due to autofluorescence, thereby validating the presence of genuine GFP leakage.

Subsequently, in the homozygous fundus, we identified a distinct circular image. To investigate this further, we utilized OCT imaging. The results of OCT imaging show a breakdown in the optic nerve. Therefore, we thought that this mouse model might mimic glaucoma. There are two important aspects for the disorder glaucoma increased IOP pressure and RGC loss. Therefore, we measured intraocular pressure (IOP) as part of our analysis. However, the IOP result did not show any significant difference between the three genotypes. The disorder NTG also does not show any elevated IOP, which are related to mutations of *Optn and Tbk1*. [53][63]. It was critical to assess the viability of retinal cells to determine if cell death was occurring which might relate the phenotype we observed to NTG. Therefore, we experimented on gene expression related to RGCs since RGC loss is a significant factor in glaucoma disorder. However, no significant cell death of RGCs was detected in our experiments with ddPCR. Interestingly, *Melanopsin* transcription on Pou4f2$^{AP/AP}$ animals were decreased compared to the other three genotypes however the level of reduction is not as severe as *Pou4f1* and *NfL* transcription. Since *Melanopsin* is a photopigment expressed in the ipRGCs maybe ipRGCs are not as significantly affected as the other RGC populations in the Pou4f2$^{AP/AP}$ knockout retina. The reason for that might be ipRGCs are more resistant than other RGC populations. Transcription of *Melanopsin* did not show any significant difference between three genotypes of dCas9-SPH. *Rhodopsin* transcription on the Pou4f2$^{AP/AP}$ animals were almost completely eliminated. This is an interesting finding and suggests that RGC loss in Pou4f2$^{AP/AP}$ animals interferes with the neuronal signaling, resulting in reduced rhodopsin expression in Pou4f2$^{AP/AP}$ retinas. The developers of the Pou4f2$^{AP/AP}$ mouse model experimented for RGC markers. However, no expression difference was reported for the *Melanopsin* and *Rhodopsin*. Another finding of ours is that the mice with homozygous genotype displayed a

rotational movement and some displayed developmental delays which further suggests that the cupping we observed might be neuronal origin and effect other types of neuronal genes as well.

Furthermore, The Jackson Laboratory reported that the transgene insertion site of dCas9-SPH animals is at intron 3 of the Dpysl2 gene on chromosome 14 [147], in contrast to the Gm33925 on chromosome 3 reported by the originating article [115]. Based on this information, we hypothesized that the underlying issue for the observed phenotype might be related to the *Dpysl2* gene, which is affirmative with our findings because of the observed circular movement phenotype in dCas9-SPH$^{ki/ki}$ genotype.

Our experiments showed that there is only one insertion in our animals and the insertion is on chromosome 14. Moreover, the insertion found in chromosome 14 is in the *Dpysl2* gene which supports our hypothesis on the neuronal origin of the phenotype. *Dpysl2* gene is associated with axonal transport and is known as a neuronal gene. Therefore, we experimented on *Dpysl2* gene with designed primers to detect the *Dpysl2* transcripts. Our ddPCR data confirmed that the insertion on the chromosome 14 led to *Dpysl2* gene knockdown considering the linear reduction between, dCas9-SPH$^{wt/wt}$, dCas9-SPH$^{ki/wt}$ and dCas9-SPH$^{ki/ki}$ animals respectively. Even though *Dpysl2* transcripts were present in dCas9-SPH$^{ki/ki}$ animals, their levels were severely reduced. This indicates that the gene is unable to undergo proper splicing. This information about *Dpysl2* gene transcription between our three genotypes lead us to hypothesize that the observed phenotype is neurological and the reason for it is *Dpysl2* gene knockdown. These findings suggest that the observed phenotype could serve as a hereditary model for optic cupping, likely driven by the knockdown of *Dpysl2* gene.

In another study, researchers block the translation of *Crmp2* in zebra fish. Their data showed that *Crmp2* knock down induces growth defects in retinal axons [148]. Future studies related to our

experiments could focus on evaluating the axonal growth in these transgenic animals. Another study was performed with a *Crmp2* deficient generated mice. Researchers wanted to found the role of *Crmp2* in the cerebral cortex. Their data showed that there was a reduction in the density of dendritic spines without any defects for dendritic patterning phenotype in the *Crmp2* deficient mouse. Even though they did not check the eye, they reported that the *Crmp2* deficient animals were grossly normal in size, development, growth, general behavior and appearance [149]. However, in some of the dCas9-SPH homozygous knock in animals we observed circular movement and developmental delays. In another brain specific study, researchers create a *Crmp2* knock out mouse model. Their data showed a variable degree of lateral ventricle enlargement in *Crmp2* knock out mouse which was similar seen on the schizophrenia patients. On a behavioral aspect, the transgenic animals displayed an increased locomotion compared to the control animals. They reported that *Crmp2* dysfunction has an important role in the expression of several behavioral impairments and structural abnormalities [150]. Even though the study did not contain data on the eye aspect of the animals, behavioral abnormalities are similar to our findings.

GFP leakage is observed both in heterozygote and homozygote knock in animals. In contrast, optic cupping only happens in the dCas9-SPH$^{ki/ki}$ animals and not in other two genotypes therefore, the knock in allele, dCas9-SPH for the *Dpysl2* gene must be recessive. More interestingly, the optic cupping phenotype did not show any IOP upregulation or RGC loss which suggested an asymptomatic bilateral structural defect. This is in contrast to the morning glory syndrome which usually appear in only one eye. The dCas9-SPH$^{ki/ki}$ transgenic animal is unique in that respect and can be used as an informative model for hereditary optic cupping and as a *Dpysl2* gene knockdown.

5. BIBLIOGRAPHY

1. Ptito, M., M. Bleau, and J. Bouskila, *The Retina: A Window into the Brain.* Cells, 2021. **10**(12).
2. Meek, K.M. and C. Knupp, *Corneal structure and transparency.* Prog Retin Eye Res, 2015. **49**: p. 1-16.
3. Galindo-Romero, C., et al., *The retina of the lab rat: focus on retinal ganglion cells and photoreceptors.* Front Neuroanat, 2022. **16**: p. 994890.
4. Mahabadi, N. and Y. Al Khalili, *Neuroanatomy, Retina*, in *StatPearls*. 2024: Treasure Island (FL).
5. Batista, A., et al., *Normative mice retinal thickness: 16-month longitudinal characterization of wild-type mice and changes in a model of Alzheimer's disease.* Front Aging Neurosci, 2023. **15**: p. 1161847.
6. Hong, Y.K., I.J. Kim, and J.R. Sanes, *Stereotyped axonal arbors of retinal ganglion cell subsets in the mouse superior colliculus.* J Comp Neurol, 2011. **519**(9): p. 1691-711.
7. Young, M.J. and R.D. Lund, *The retinal ganglion cells that drive the pupilloconstrictor response in rats.* Brain Res, 1998. **787**(2): p. 191-202.
8. Struebing, F.L., et al., *Genetic Networks in Mouse Retinal Ganglion Cells.* Front Genet, 2016. **7**: p. 169.
9. Garraghty, P.E. and M. Sur, *Competitive interactions influencing the development of retinal axonal arbors in cat lateral geniculate nucleus.* Physiol Rev, 1993. **73**(3): p. 529-45.
10. Wassle, H. and B.B. Boycott, *Functional architecture of the mammalian retina.* Physiol Rev, 1991. **71**(2): p. 447-80.
11. Yamagata, M. and J.R. Sanes, *Lamina-specific cues guide outgrowth and arborization of retinal axons in the optic tectum.* Development, 1995. **121**(1): p. 189-200.
12. Yamagata, M. and J.R. Sanes, *Target-independent diversification and target-specific projection of chemically defined retinal ganglion cell subsets.* Development, 1995. **121**(11): p. 3763-76.
13. Sernagor, E., S.J. Eglen, and R.O. Wong, *Development of retinal ganglion cell structure and function.* Prog Retin Eye Res, 2001. **20**(2): p. 139-74.
14. Weinreb, R.N., T. Aung, and F.A. Medeiros, *The pathophysiology and treatment of glaucoma: a review.* JAMA, 2014. **311**(18): p. 1901-11.
15. Howell, G.R., et al., *Axons of retinal ganglion cells are insulted in the optic nerve early in DBA/2J glaucoma.* J Cell Biol, 2007. **179**(7): p. 1523-37.
16. Caprioli, J. and R. Varma, *Intraocular pressure: modulation as treatment for glaucoma.* Am J Ophthalmol, 2011. **152**(3): p. 340-344 e2.
17. Almasieh, M., et al., *The molecular basis of retinal ganglion cell death in glaucoma.* Prog Retin Eye Res, 2012. **31**(2): p. 152-81.
18. Kaur, G. and N.K. Singh, *Inflammation and retinal degenerative diseases.* Neural Regen Res, 2023. **18**(3): p. 513-518.
19. Rein, D.B., et al., *The Economic Burden of Vision Loss and Blindness in the United States.* Ophthalmology, 2022. **129**(4): p. 369-378.

20. in *Webvision: The Organization of the Retina and Visual System*, H. Kolb, et al., Editors. 1995: Salt Lake City (UT).
21. Landau, K. and M. Kurz-Levin, *Retinal disorders.* Handb Clin Neurol, 2011. **102**: p. 97-116.
22. Wong, W.L., et al., *Global prevalence of age-related macular degeneration and disease burden projection for 2020 and 2040: a systematic review and meta-analysis.* Lancet Glob Health, 2014. **2**(2): p. e106-16.
23. Martinez-Aguila, A., et al., *Influence of Circadian Rhythm in the Eye: Significance of Melatonin in Glaucoma.* Biomolecules, 2021. **11**(3).
24. Antonetti, D.A., R. Klein, and T.W. Gardner, *Diabetic retinopathy.* N Engl J Med, 2012. **366**(13): p. 1227-39.
25. Wilkinson, C.P., et al., *Proposed international clinical diabetic retinopathy and diabetic macular edema disease severity scales.* Ophthalmology, 2003. **110**(9): p. 1677-82.
26. Friedman, D.S., et al., *Prevalence of age-related macular degeneration in the United States.* Arch Ophthalmol, 2004. **122**(4): p. 564-72.
27. Ambati, J. and B.J. Fowler, *Mechanisms of age-related macular degeneration.* Neuron, 2012. **75**(1): p. 26-39.
28. Dias, M.F., et al., *Molecular genetics and emerging therapies for retinitis pigmentosa: Basic research and clinical perspectives.* Prog Retin Eye Res, 2018. **63**: p. 107-131.
29. Nguyen, X.T., et al., *Retinitis Pigmentosa: Current Clinical Management and Emerging Therapies.* Int J Mol Sci, 2023. **24**(8).
30. Brunet, A.A., A.R. Harvey, and L.S. Carvalho, *Primary and Secondary Cone Cell Death Mechanisms in Inherited Retinal Diseases and Potential Treatment Options.* Int J Mol Sci, 2022. **23**(2).
31. Quigley, H.A., *Number of people with glaucoma worldwide.* Br J Ophthalmol, 1996. **80**(5): p. 389-93.
32. Schuster, A.K., et al., *The Diagnosis and Treatment of Glaucoma.* Dtsch Arztebl Int, 2020. **117**(13): p. 225-234.
33. Della Santina, L., et al., *Differential progression of structural and functional alterations in distinct retinal ganglion cell types in a mouse model of glaucoma.* J Neurosci, 2013. **33**(44): p. 17444-57.
34. Fernandes, K.A., et al., *Using genetic mouse models to gain insight into glaucoma: Past results and future possibilities.* Exp Eye Res, 2015. **141**: p. 42-56.
35. John, S.W., et al., *Essential iris atrophy, pigment dispersion, and glaucoma in DBA/2J mice.* Invest Ophthalmol Vis Sci, 1998. **39**(6): p. 951-62.
36. Overby, D.R., et al., *Altered mechanobiology of Schlemm's canal endothelial cells in glaucoma.* Proc Natl Acad Sci U S A, 2014. **111**(38): p. 13876-81.
37. Zode, G.S., et al., *Reduction of ER stress via a chemical chaperone prevents disease phenotypes in a mouse model of primary open angle glaucoma.* J Clin Invest, 2011. **121**(9): p. 3542-53.
38. Nickells, R.W., et al., *Under pressure: cellular and molecular responses during glaucoma, a common neurodegeneration with axonopathy.* Annu Rev Neurosci, 2012. **35**: p. 153-79.
39. May, C.A. and E. Lutjen-Drecoll, *Morphology of the murine optic nerve.* Invest Ophthalmol Vis Sci, 2002. **43**(7): p. 2206-12.

40. Downs, J.C., M.D. Roberts, and C.F. Burgoyne, *Mechanical environment of the optic nerve head in glaucoma.* Optom Vis Sci, 2008. **85**(6): p. 425-35.
41. Morrison, J.C., W.O. Cepurna, and E.C. Johnson, *Modeling glaucoma in rats by sclerosing aqueous outflow pathways to elevate intraocular pressure.* Exp Eye Res, 2015. **141**: p. 23-32.
42. Waisberg, E. and J.A. Micieli, *Neuro-Ophthalmological Optic Nerve Cupping: An Overview.* Eye Brain, 2021. **13**: p. 255-268.
43. Quigley, H.A. and W.R. Green, *The Histology of Human Glaucoma Cupping and Optic Nerve Damage: Clinicopathologic Correlation in 21 Eyes.* Ophthalmology, 2020. **127**(4S): p. S45-S69.
44. Trobe, J.D., et al., *Nonglaucomatous excavation of the optic disc.* Arch Ophthalmol, 1980. **98**(6): p. 1046-50.
45. Cheng, J.W., et al., *Myocilin polymorphisms and primary open-angle glaucoma: a systematic review and meta-analysis.* PLoS One, 2012. **7**(9): p. e46632.
46. Stone, E.M., et al., *Identification of a gene that causes primary open angle glaucoma.* Science, 1997. **275**(5300): p. 668-70.
47. Katoli, P., et al., *Full-length myocilin protein is purified from mammalian cells as a dimer.* Protein Expr Purif, 2018. **147**: p. 38-48.
48. Faralli, J.A., et al., *NFATc1 activity regulates the expression of myocilin induced by dexamethasone.* Exp Eye Res, 2015. **130**: p. 9-16.
49. Qiu, Y., et al., *Cellular processing of myocilin.* PLoS One, 2014. **9**(4): p. e92845.
50. Wang, H., et al., *Physiological function of myocilin and its role in the pathogenesis of glaucoma in the trabecular meshwork (Review).* Int J Mol Med, 2019. **43**(2): p. 671-681.
51. Leung, Y.F., et al., *Different optineurin mutation pattern in primary open-angle glaucoma.* Invest Ophthalmol Vis Sci, 2003. **44**(9): p. 3880-4.
52. Swarup, G. and Z. Sayyad, *Altered Functions and Interactions of Glaucoma-Associated Mutants of Optineurin.* Front Immunol, 2018. **9**: p. 1287.
53. Rezaie, T., et al., *Adult-onset primary open-angle glaucoma caused by mutations in optineurin.* Science, 2002. **295**(5557): p. 1077-9.
54. Minegishi, Y., et al., *Significance of optineurin mutations in glaucoma and other diseases.* Prog Retin Eye Res, 2016. **55**: p. 149-181.
55. Chi, Z.L., et al., *Overexpression of optineurin E50K disrupts Rab8 interaction and leads to a progressive retinal degeneration in mice.* Hum Mol Genet, 2010. **19**(13): p. 2606-15.
56. Minegishi, Y., et al., *Enhanced optineurin E50K-TBK1 interaction evokes protein insolubility and initiates familial primary open-angle glaucoma.* Hum Mol Genet, 2013. **22**(17): p. 3559-67.
57. Tseng, H.C., et al., *Visual impairment in an optineurin mouse model of primary open-angle glaucoma.* Neurobiol Aging, 2015. **36**(6): p. 2201-12.
58. Sarfarazi, M. and I. Stoilov, *Molecular genetics of primary congenital glaucoma.* Eye (Lond), 2000. **14 (Pt 3B)**: p. 422-8.
59. MacKinnon, J.R., et al., *Primary infantile glaucoma in an Australian population.* Clin Exp Ophthalmol, 2004. **32**(1): p. 14-8.
60. Duester, G., *Keeping an eye on retinoic acid signaling during eye development.* Chem Biol Interact, 2009. **178**(1-3): p. 178-81.
61. Cvekl, A. and W.L. Wang, *Retinoic acid signaling in mammalian eye development.* Exp Eye Res, 2009. **89**(3): p. 280-91.

62. Mookherjee, S., et al., *Molecular basis for involvement of CYP1B1 in MYOC upregulation and its potential implication in glaucoma pathogenesis.* PLoS One, 2012. **7**(9): p. e45077.
63. Morton, S., et al., *Enhanced binding of TBK1 by an optineurin mutant that causes a familial form of primary open angle glaucoma.* FEBS Lett, 2008. **582**(6): p. 997-1002.
64. Fingert, J.H., et al., *Copy number variations on chromosome 12q14 in patients with normal tension glaucoma.* Hum Mol Genet, 2011. **20**(12): p. 2482-94.
65. Fingert, J.H., et al., *Transgenic TBK1 mice have features of normal tension glaucoma.* Hum Mol Genet, 2017. **26**(1): p. 124-132.
66. Ye, M., et al., *TBK1 Knockdown Alleviates Axonal Transport Deficits in Retinal Ganglion Cells Via mTORC1 Activation in a Retinal Damage Mouse Model.* Invest Ophthalmol Vis Sci, 2023. **64**(10): p. 1.
67. Ritch, R., et al., *TBK1 gene duplication and normal-tension glaucoma.* JAMA Ophthalmol, 2014. **132**(5): p. 544-8.
68. Monemi, S., et al., *Identification of a novel adult-onset primary open-angle glaucoma (POAG) gene on 5q22.1.* Hum Mol Genet, 2005. **14**(6): p. 725-33.
69. Gallenberger, M., et al., *Lack of WDR36 leads to preimplantation embryonic lethality in mice and delays the formation of small subunit ribosomal RNA in human cells in vitro.* Hum Mol Genet, 2011. **20**(3): p. 422-35.
70. Skarie, J.M. and B.A. Link, *The primary open-angle glaucoma gene WDR36 functions in ribosomal RNA processing and interacts with the p53 stress-response pathway.* Hum Mol Genet, 2008. **17**(16): p. 2474-85.
71. Blanco-Marchite, C., et al., *WDR36 and P53 gene variants and susceptibility to primary open-angle glaucoma: analysis of gene-gene interactions.* Invest Ophthalmol Vis Sci, 2011. **52**(11): p. 8467-78.
72. Altay, H.Y., et al., *Gene regulatory and gene editing tools and their applications for retinal diseases and neuroprotection: From proof-of-concept to clinical trial.* Front Neurosci, 2022. **16**: p. 924917.
73. Jain, A., et al., *CRISPR-Cas9-based treatment of myocilin-associated glaucoma.* Proc Natl Acad Sci U S A, 2017. **114**(42): p. 11199-11204.
74. Steinkuller, P.G., *The morning glory disk anomaly: case report and literature review.* J Pediatr Ophthalmol Strabismus, 1980. **17**(2): p. 81-7.
75. Jackson, W.E. and S. Freed, *Ocular and systemic abnormalities associated with morning glory syndrome.* Ophthalmic Paediatr Genet, 1985. **5**(1-2): p. 111-5.
76. Jacobs, M. and D. Taylor, *The systemic and genetic significance of congenital optic disc anomalies.* Eye (Lond), 1991. **5 (Pt 4)**: p. 470-5.
77. Manschot, W.A., *Morning glory syndrome: a histopathological study.* Br J Ophthalmol, 1990. **74**(1): p. 56-8.
78. Cong, L., et al., *Multiplex genome engineering using CRISPR/Cas systems.* Science, 2013. **339**(6121): p. 819-23.
79. Jinek, M., et al., *A programmable dual-RNA-guided DNA endonuclease in adaptive bacterial immunity.* Science, 2012. **337**(6096): p. 816-21.
80. Doudna, J.A. and E. Charpentier, *Genome editing. The new frontier of genome engineering with CRISPR-Cas9.* Science, 2014. **346**(6213): p. 1258096.
81. Qi, L.S., et al., *Repurposing CRISPR as an RNA-guided platform for sequence-specific control of gene expression.* Cell, 2013. **152**(5): p. 1173-83.

82. Ziccardi, L., et al., *Gene Therapy in Retinal Dystrophies.* Int J Mol Sci, 2019. **20**(22).
83. Ong, T., et al., *Adeno-Associated Viral Gene Therapy for Inherited Retinal Disease.* Pharm Res, 2019. **36**(2): p. 34.
84. Niu, J., B. Zhang, and H. Chen, *Applications of TALENs and CRISPR/Cas9 in human cells and their potentials for gene therapy.* Mol Biotechnol, 2014. **56**(8): p. 681-8.
85. Garneau, J.E., et al., *The CRISPR/Cas bacterial immune system cleaves bacteriophage and plasmid DNA.* Nature, 2010. **468**(7320): p. 67-71.
86. Mali, P., et al., *RNA-guided human genome engineering via Cas9.* Science, 2013. **339**(6121): p. 823-6.
87. Mali, P., et al., *CAS9 transcriptional activators for target specificity screening and paired nickases for cooperative genome engineering.* Nat Biotechnol, 2013. **31**(9): p. 833-8.
88. Sapranauskas, R., et al., *The Streptococcus thermophilus CRISPR/Cas system provides immunity in Escherichia coli.* Nucleic Acids Res, 2011. **39**(21): p. 9275-82.
89. Gilbert, L.A., et al., *CRISPR-mediated modular RNA-guided regulation of transcription in eukaryotes.* Cell, 2013. **154**(2): p. 442-51.
90. Maeder, M.L., et al., *CRISPR RNA-guided activation of endogenous human genes.* Nat Methods, 2013. **10**(10): p. 977-9.
91. Perez-Pinera, P., et al., *RNA-guided gene activation by CRISPR-Cas9-based transcription factors.* Nat Methods, 2013. **10**(10): p. 973-6.
92. Chavez, A., et al., *Highly efficient Cas9-mediated transcriptional programming.* Nat Methods, 2015. **12**(4): p. 326-8.
93. Wagner, D.L., et al., *High prevalence of Streptococcus pyogenes Cas9-reactive T cells within the adult human population.* Nat Med, 2019. **25**(2): p. 242-248.
94. Gaj, T., C.A. Gersbach, and C.F. Barbas, 3rd, *ZFN, TALEN, and CRISPR/Cas-based methods for genome engineering.* Trends Biotechnol, 2013. **31**(7): p. 397-405.
95. Kandavelou, K. and S. Chandrasegaran, *Custom-designed molecular scissors for site-specific manipulation of the plant and mammalian genomes.* Methods Mol Biol, 2009. **544**: p. 617-36.
96. Kim, Y.G., et al., *Site-specific cleavage of DNA-RNA hybrids by zinc finger/FokI cleavage domain fusions.* Gene, 1997. **203**(1): p. 43-9.
97. Miller, J.C., et al., *An improved zinc-finger nuclease architecture for highly specific genome editing.* Nat Biotechnol, 2007. **25**(7): p. 778-85.
98. Porteus, M., *Design and testing of zinc finger nucleases for use in mammalian cells.* Methods Mol Biol, 2008. **435**: p. 47-61.
99. Santiago, Y., et al., *Targeted gene knockout in mammalian cells by using engineered zinc-finger nucleases.* Proc Natl Acad Sci U S A, 2008. **105**(15): p. 5809-14.
100. Shukla, V.K., et al., *Precise genome modification in the crop species Zea mays using zinc-finger nucleases.* Nature, 2009. **459**(7245): p. 437-41.
101. Szczepek, M., et al., *Structure-based redesign of the dimerization interface reduces the toxicity of zinc-finger nucleases.* Nat Biotechnol, 2007. **25**(7): p. 786-93.
102. Remy, S., et al., *Zinc-finger nucleases: a powerful tool for genetic engineering of animals.* Transgenic Res, 2010. **19**(3): p. 363-71.
103. Beerli, R.R. and C.F. Barbas, 3rd, *Engineering polydactyl zinc-finger transcription factors.* Nat Biotechnol, 2002. **20**(2): p. 135-41.
104. Pabo, C.O., E. Peisach, and R.A. Grant, *Design and selection of novel Cys2His2 zinc finger proteins.* Annu Rev Biochem, 2001. **70**: p. 313-40.

105. Urnov, F.D., et al., *Genome editing with engineered zinc finger nucleases.* Nat Rev Genet, 2010. **11**(9): p. 636-46.
106. Boch, J., et al., *Breaking the code of DNA binding specificity of TAL-type III effectors.* Science, 2009. **326**(5959): p. 1509-12.
107. Bogdanove, A.J., S. Schornack, and T. Lahaye, *TAL effectors: finding plant genes for disease and defense.* Curr Opin Plant Biol, 2010. **13**(4): p. 394-401.
108. Moscou, M.J. and A.J. Bogdanove, *A simple cipher governs DNA recognition by TAL effectors.* Science, 2009. **326**(5959): p. 1501.
109. Christian, M., et al., *Targeting DNA double-strand breaks with TAL effector nucleases.* Genetics, 2010. **186**(2): p. 757-61.
110. Miller, J.C., et al., *A TALE nuclease architecture for efficient genome editing.* Nat Biotechnol, 2011. **29**(2): p. 143-8.
111. Li, T., et al., *TAL nucleases (TALNs): hybrid proteins composed of TAL effectors and FokI DNA-cleavage domain.* Nucleic Acids Res, 2011. **39**(1): p. 359-72.
112. Makarova, K.S. and E.V. Koonin, *Annotation and Classification of CRISPR-Cas Systems.* Methods Mol Biol, 2015. **1311**: p. 47-75.
113. Kim, D., et al., *Digenome-seq: genome-wide profiling of CRISPR-Cas9 off-target effects in human cells.* Nat Methods, 2015. **12**(3): p. 237-43, 1 p following 243.
114. Chavez, A., et al., *Comparison of Cas9 activators in multiple species.* Nat Methods, 2016. **13**(7): p. 563-567.
115. Zhou, H., et al., *In vivo simultaneous transcriptional activation of multiple genes in the brain using CRISPR-dCas9-activator transgenic mice.* Nat Neurosci, 2018. **21**(3): p. 440-446.
116. Gan, L., et al., *POU domain factor Brn-3b is essential for retinal ganglion cell differentiation and survival but not for initial cell fate specification.* Dev Biol, 1999. **210**(2): p. 469-80.
117. Sultan, M.B., S.L. Mansberger, and P.P. Lee, *Understanding the importance of IOP variables in glaucoma: a systematic review.* Surv Ophthalmol, 2009. **54**(6): p. 643-62.
118. Mu, X., et al., *Gene regulation logic in retinal ganglion cell development: Isl1 defines a critical branch distinct from but overlapping with Pou4f2.* Proc Natl Acad Sci U S A, 2008. **105**(19): p. 6942-7.
119. Pan, L., et al., *ISL1 and BRN3B co-regulate the differentiation of murine retinal ganglion cells.* Development, 2008. **135**(11): p. 1981-90.
120. Lee, J.S., et al., *No association between POU4F1, POU4F2, ISL1 polymorphisms and normal-tension glaucoma.* Ophthalmic Genet, 2020. **41**(5): p. 427-431.
121. Subramanian, M.L., et al., *Neurofilament light chain in the vitreous humor of the eye.* Alzheimers Res Ther, 2020. **12**(1): p. 111.
122. Palczewski, K., et al., *Crystal structure of rhodopsin: A G protein-coupled receptor.* Science, 2000. **289**(5480): p. 739-45.
123. Yuasa-Kawada, J., et al., *Axonal morphogenesis controlled by antagonistic roles of two CRMP subtypes in microtubule organization.* Eur J Neurosci, 2003. **17**(11): p. 2329-43.
124. Wang, L.H. and S.M. Strittmatter, *A family of rat CRMP genes is differentially expressed in the nervous system.* J Neurosci, 1996. **16**(19): p. 6197-207.
125. Fukada, M., et al., *Molecular characterization of CRMP5, a novel member of the collapsin response mediator protein family.* J Biol Chem, 2000. **275**(48): p. 37957-65.

126. Suzuki, H., et al., *De novo non-synonymous DPYSL2 (CRMP2) variants in two patients with intellectual disabilities and documentation of functional relevance through zebrafish rescue and cellular transfection experiments.* Hum Mol Genet, 2022. **31**(24): p. 4173-4182.
127. Brot, S., et al., *CRMP5 interacts with tubulin to inhibit neurite outgrowth, thereby modulating the function of CRMP2.* J Neurosci, 2010. **30**(32): p. 10639-54.
128. Yamashita, N., et al., *Regulation of spine development by semaphorin3A through cyclin-dependent kinase 5 phosphorylation of collapsin response mediator protein 1.* J Neurosci, 2007. **27**(46): p. 12546-54.
129. Arimura, N., et al., *Phosphorylation by Rho kinase regulates CRMP-2 activity in growth cones.* Mol Cell Biol, 2005. **25**(22): p. 9973-84.
130. Goshima, Y., et al., *Collapsin-induced growth cone collapse mediated by an intracellular protein related to UNC-33.* Nature, 1995. **376**(6540): p. 509-14.
131. Uchida, Y., et al., *Semaphorin3A signaling mediated by Fyn-dependent tyrosine phosphorylation of collapsin response mediator protein 2 at tyrosine 32.* J Biol Chem, 2009. **284**(40): p. 27393-401.
132. Yoshimura, T., et al., *GSK-3beta regulates phosphorylation of CRMP-2 and neuronal polarity.* Cell, 2005. **120**(1): p. 137-49.
133. Yamashita, N., et al., *CRMP5 (collapsin response mediator protein 5) regulates dendritic development and synaptic plasticity in the cerebellar Purkinje cells.* J Neurosci, 2011. **31**(5): p. 1773-9.
134. Yamashita, N., et al., *Collapsin response mediator protein 1 mediates reelin signaling in cortical neuronal migration.* J Neurosci, 2006. **26**(51): p. 13357-62.
135. Silva, P.N., et al., *CNP and DPYSL2 mRNA expression and promoter methylation levels in brain of Alzheimer's disease patients.* J Alzheimers Dis, 2013. **33**(2): p. 349-55.
136. Numata-Uematsu, Y., et al., *Inhibition of collapsin response mediator protein-2 phosphorylation ameliorates motor phenotype of ALS model mice expressing SOD1G93A.* Neurosci Res, 2019. **139**: p. 63-68.
137. White, K.A., et al., *Modulation of CRMP2 via (S)-Lacosamide shows therapeutic promise but is ultimately ineffective in a mouse model of CLN6-Batten disease.* Neuronal Signal, 2019. **3**(2): p. NS20190001.
138. Brustovetsky, T., R. Khanna, and N. Brustovetsky, *Involvement of CRMP2 in Regulation of Mitochondrial Morphology and Motility in Huntington's Disease.* Cells, 2021. **10**(11).
139. Izumi, R., et al., *Dysregulation of DPYSL2 expression by mTOR signaling in schizophrenia: Multi-level study of postmortem brain.* Neurosci Res, 2022. **175**: p. 73-81.
140. Khanna, R., et al., *Opening Pandora's jar: a primer on the putative roles of CRMP2 in a panoply of neurodegenerative, sensory and motor neuron, and central disorders.* Future Neurol, 2012. **7**(6): p. 749-771.
141. Liu, Y., et al., *Functional variants in DPYSL2 sequence increase risk of schizophrenia and suggest a link to mTOR signaling.* G3 (Bethesda), 2014. **5**(1): p. 61-72.
142. Pham, X., et al., *The DPYSL2 gene connects mTOR and schizophrenia.* Transl Psychiatry, 2016. **6**(11): p. e933.
143. Yoshihara, S., et al., *Betaine ameliorates schizophrenic traits by functionally compensating for KIF3-based CRMP2 transport.* Cell Rep, 2021. **35**(2): p. 108971.

144. Fallin, M.D., et al., *Bipolar I disorder and schizophrenia: a 440-single-nucleotide polymorphism screen of 64 candidate genes among Ashkenazi Jewish case-parent trios.* Am J Hum Genet, 2005. **77**(6): p. 918-36.
145. Fallin, M.D., et al., *Linkage and association on 8p21.2-p21.1 in schizophrenia.* Am J Med Genet B Neuropsychiatr Genet, 2011. **156**(2): p. 188-97.
146. Wang, Z., et al., *Axon guidance pathway genes are associated with schizophrenia risk.* Exp Ther Med, 2018. **16**(6): p. 4519-4526.
147. Laboratory, T.J. *B6;D2-Tn(pb-CAG-cas9*,-EGFP)1Yangh/J*. 2022; Available from: https://www.jax.org/strain/031645.
148. Liu, Z.Z., et al., *CRMP2 and CRMP4 Are Differentially Required for Axon Guidance and Growth in Zebrafish Retinal Neurons.* Neural Plast, 2018. **2018**: p. 8791304.
149. Makihara, H., et al., *CRMP1 and CRMP2 have synergistic but distinct roles in dendritic development.* Genes Cells, 2016. **21**(9): p. 994-1005.
150. Zhang, H., et al., *Brain-specific Crmp2 deletion leads to neuronal development deficits and behavioural impairments in mice.* Nat Commun, 2016. **7**.